Chrna5 and lynx prototoxins identify acetylcholine super-responder subplate neurons

Sridevi Venkatesan[1], Tianhui Chen[1], Yupeng Liu[1], Eric E Turner[2], Shreejoy Tripathy[1,3,4,5], *Evelyn K Lambe[1,4,6]

1. Department of Physiology, Temerty Faculty of Medicine, University of Toronto, Toronto ON, Canada
2. Center for Integrative Brain Research, Seattle Children's Research Institute, Seattle WA, USA
3. Krembil Centre for Neuroinformatics, Centre for Addiction and Mental Health, Toronto ON, Canada
4. Department of Psychiatry, University of Toronto, Toronto ON, Canada
5. Institute of Medical Science, University of Toronto, Toronto ON, Canada
6. Department of Obstetrics and Gynecology, University of Toronto, Toronto ON, Canada

Corresponding author:
E.K. Lambe, Ph.D.
1 King's College Circle
Toronto ON
Canada M5S 1A8
(416) 946-0910
Email: evelyn.lambe@utoronto.ca

Summary (150 words)

Attention depends on cholinergic excitation of prefrontal neurons but is sensitive to perturbation of α5-containing nicotinic receptors encoded by *Chrna5*. However, *Chrna5*-expressing (Chrna5+) neurons remain enigmatic, despite their potential as a target to improve attention. Here, we generate complex transgenic mice to probe Chrna5+ neurons and their sensitivity to endogenous acetylcholine. Through opto-physiological experiments, we discover that Chrna5+ neurons contain a distinct population of acetylcholine super-responders. Leveraging single-cell transcriptomics, we discover molecular markers conferring subplate identity on this subset. We determine that Chrna5+ super-responders express a unique complement of GPI-anchored lynx prototoxin genes (*Lypd1*, *Ly6g6e*, and *Lypd6b*), predicting distinct nicotinic receptor regulation. To manipulate lynx regulation of endogenous nicotinic responses, we developed a pharmacological strategy guided by transcriptomic predictions. Overall, we reveal *Chrna5*-Cre mice as a transgenic tool to target the diversity of subplate neurons in adulthood, yielding new molecular strategies to manipulate their cholinergic activation relevant to attention disorders.

Keywords

Acetylcholine, Chrna5, nicotinic receptor, alpha5, prefrontal cortex, subplate, lynx prototoxins, transcriptomics, optogenetics, electrophysiology

Introduction (723 words)

Cholinergic modulation of the medial prefrontal cortex (mPFC) is essential for attention and detection of sensory cues (Dalley et al., 2004b, 2004a; Gritton et al., 2016; McGaughy et al., 2002). Deep-layer pyramidal neurons in the PFC are critically involved in such executive function (Briggs and Usrey, 2008; Spellman et al., 2021; Voigts et al., 2020) and are robustly excited by acetylcholine (Kassam et al., 2008; Sparks et al., 2018), via nicotinic and muscarinic receptor activation (Venkatesan et al., 2020). The α5 nicotinic receptor subunit encoded by *Chrna5* is specifically expressed in deep-layer pyramidal neurons (Wada et al., 1990; Winzer-Serhan and Leslie, 2005), forming high-affinity nicotinic receptors in combination with α4 and β2 subunits. Electrophysiological, behavioural, and genetic evidence in both rodents and humans point to an important role of *Chrna5* expression for nicotinic receptor function, attention, and executive function.

Constitutive deletion of *Chrna5* in mice, or knockdown in the adult rat PFC disrupt attention and reduce nicotinic receptor activation by exogenous acetylcholine stimulation in layer 6 neurons (Bailey et al., 2010; Howe et al., 2018a; Tian et al., 2011). Optogenetic experiments in *Chrna5*$^{-/-}$ mice show that *Chrna5* is required for rapid onset of postsynaptic cholinergic activation and prevents desensitization of the endogenous cholinergic response during prolonged stimulation (Venkatesan and Lambe, 2020). In humans, the non-synonymous rs16969968 (D398N) polymorphism in *Chrna5* is associated with nicotine dependence, schizophrenia and cognitive impairment (Bierut et al., 2008; Han et al., 2019; Schuch et al., 2016). Nicotinic α4β2α5 receptors with the D398N polymorphism have partial loss of function, attributed to changes in receptor desensitization, calcium permeability, or membrane trafficking (Maskos, 2020; Prevost et al., 2020; Scholze and Huck, 2020).

Despite α5 nicotinic receptor involvement in attention and prefrontal cholinergic activation, systematic characterization of *Chrna5*-expressing neurons using modern genetic tools is lacking. Deep-layer neurons include diverse corticothalamic (L6CT), corticocortical, and layer 6b (L6b) populations (Briggs, 2010; Sorensen et al., 2015; Thomson, 2010). *Chrna5* is predicted to be expressed in L6CT neurons (Heath et al., 2010; Kassam et al., 2008), which are usually identified by their expression of *Syt6*, a conserved L6CT neuronal marker (Harris et al., 2014, 2019; Nectow et al., 2017a). *Syt6*-Cre mice have been widely used to characterize prefrontal L6CT neurons and their cholinergic properties (Nakayama et al., 2018; Tian et al., 2014; Vaasjo et al., 2021). However, it is unclear whether these are the same neurons expressing *Chrna5*. Characterization of *Chrna5*-expressing neurons has been limited by the lack of verified antibodies for the α5 subunit that could be used for post-hoc immunostaining. Previous BAC-transgenic mice labeling *Chrna5*-expressing neurons had altered expression of other genes in the tightly linked *Chrna5/a3/b4* gene cluster, limiting their use for functional examination (Ables et al., 2017). This issue was circumvented by disrupting the open reading frames of *Chrna3/b4* in the BAC transgene to generate a *Chrna5*-Cre mouse without misexpression artifacts (Morton et al., 2018).

Here, we create compound transgenic mice to investigate how prefrontal *Chrna5*-expressing (Chrna5+) neurons respond to optogenetic release of endogenous acetylcholine. The

fast and strong response prompted a multi-approach examination of Chrna5+ neurons together with a control population of *Syt6*-expressing (Syt6+) neurons, a more traditional molecular marker of deep-layer prefrontal cortex. We demonstrate a large fraction of Chrna5+ neurons have distinctive high-affinity cholinergic responses. Single-cell RNAseq analysis reveals the expression of several subplate markers (*Cplx3*, *Ctgf*, and *Lpar1*) in this Chrna5+ subset, identifying them as subplate neurons born early in development that are critical for establishing thalamocortical connectivity (Hoerder-Suabedissen and Molnár, 2013; Kanold and Luhmann, 2010; Luhmann et al., 2018). Chrna5+ subplate neurons show distinct expression pattern of GPI-anchored lynx prototoxins (*Ly6g6e*, *Lypd1*, and *Lypd6b*) capable of exerting complex modulation of nicotinic receptor properties (Miwa et al., 2019; Wu et al., 2015). As predicted from the transcriptomic analysis, our pharmacological manipulations targeting lynx prototoxins successfully alter endogeneous nicotinic responses, revealing cell-type specific lynx regulation of nicotinic receptors.

Recent studies have examined cell-type specific modulation of nicotinic receptors by different lynx prototoxins and the consequences for cortical development and cognition (Anderson et al., 2020; Demars and Morishita, 2014; Falk et al., 2021; Miwa, 2021). Here, we discovered endogenous lynx modulation of nicotinic properties relevant for attention in subplate neurons expressing *Chrna5*. Our work highlights *Chrna5*-Cre mice as a transgenic tool to target acetylcholine super-responder subplate neurons and identifies strategies to fine-tune their cholinergic activation by manipulating GPI-anchored lynx prototoxins.

Results

Chrna5 expression identifies acetylcholine 'super-responders'

To characterize prefrontal *Chrna5*-expressing (Chrna5+) neurons, we generated triple transgenic *Chrna5*-Cre$^{/+}$Ai14$^{/+}$ChAT-ChR2$^{/+}$ mice (**Fig 1A**) and examined optogenetic cholinergic responses in labeled Chrna5+ neurons. These mice expressed tdTomato in Chrna5+ neurons and channelrhodopsin-2 in cholinergic axons as seen by two-photon imaging (**Fig 1B**). We recorded endogenous cholinergic responses in labeled Chrna5+ neurons with optophysiology in mPFC slices, using unlabeled pyramidal neurons as a control (**Fig 1C**). Optogenetic Chrna5+ neurons clearly possessed larger-amplitude cholinergic responses with significantly faster onset compared to control neurons (**Fig 1D-F**). The rising slope was significantly larger in Chrna5+ neurons (220 ± 32 pA/s, 24 cells from 4 mice) compared to control (123 ± 22 pA/s, 15 cells; $t_{(37)}$ = 2.19, P = 0.02, unpaired t-test; Cohen's d: 0.72). Similarly, peak current evoked by optogenetic acetylcholine release was greater in Chrna5+ neurons (15 ± 2 pA) compared to control (8 ± 1 pA, $t_{(37)}$ = 2.52, P = 0.02; Cohen's d: 0.83), as well as the area of the cholinergic response ($t_{(37)}$ = 2.06, P = 0.046). Intrinsic electrophysiological properties, however, did not differ between Chrna5+ and unlabeled neurons (**Suppl Table 1**). Additionally, we determined that Chrna5+ neurons are under presynaptic muscarinic autoinhibitory control, which can be relieved by atropine, resulting in even larger responses (post atropine response: 194 ± 42% of baseline, n = 6 cells). Our application of the nicotinic antagonist DHBE eliminated the optogenetic cholinergic response (post DHBE response : 3 ± 2 % of baseline, n = 4 cells), indicating the relevant

nicotinic receptors contain β2 subunits. This characterization of Chrna5+ neurons revealed them to be acetylcholine 'super-responders' with stronger and faster onset cholinergic responses distinct from other deep-layer pyramidal neurons.

To further probe the distinct cholinergic responses of prefrontal Chrna5+ neurons, we examined factors differentiating these cells from neurons labeled by *Syt6* expression (Syt6+), which has hereto been the predominant marker of layer 6 corticothalamic neurons used to characterize their function during PFC-dependent tasks (Harris et al., 2019; Nakayama et al., 2018; Nectow et al., 2017b; Vaasjo et al., 2021). Since the extent of overlap between *Chrna5* and *Syt6* expressing deep-layer pyramidal neuron populations was unclear, we adopted an imaging strategy to visualize the distribution of Chrna5+ and Syt6+ neurons in the PFC and determine the exact proportion of distinctive non-overlapping Chrna5+ neurons. We generated a compound transgenic *Chrna5*-Cre$^{/+}$Ai14$^{/+}$*Syt6*-EGFP$^{/+}$ mouse to simultaneously express tdTomato in Chrna5+ neurons and EGFP in Syt6+ neurons and performed confocal and two-photon imaging of the endogenous fluorescence of these reporters in mPFC brain slices. Chrna5+ and Syt6+ neurons were both present primarily in layer 6, with a few Chrna5+ neurons in layer 5 (**Fig 1G, I**). Closer investigation confirmed the existence of a substantial proportion of exclusively Chrna5+ neurons (37% of all labeled cells) which do not express *Syt6*, in addition to overlapping Chrna5+Syt6+ neurons (39%) which express both markers, and exclusively Syt6+ neurons (24%) which do not express *Chrna5* (N = 4 mice, **Fig 1H, J**). Thus, nearly half of all *Chrna5*-expressing neurons are not labeled by *Syt6*-expression and would have been excluded in previous studies using *Syt6*-Cre mice.

Distinct Chrna5+ neurons with highly-resilient nicotinic receptor responses

To elucidate the distinct subset of Chrna5+ neurons not found with Syt6-labeling approaches, we measured acetylcholine-evoked signals in multiple neurons simultaneously with *ex vivo* GCaMP6s Ca^{2+} imaging. We generated transgenic mice expressing GCaMP6s in either Chrna5+ (*Chrna5*-Cre$^{/+}$/Ai96$^{/+}$) or Syt6+ (*Syt6*-Cre$^{/+}$/Ai96$^{/+}$) neurons and performed two-photon imaging of mPFC layer 6 (**Fig 2A**). We measured Ca^{2+} signals evoked by acetylcholine (1 mM, 15 s) in Chrna5+ (**Suppl Video 1**) and Syt6+ neurons (**Suppl Video 2**). To pharmacologically interrogate these populations, we measured changes in the Ca^{2+} signal and proportions of acetylcholine-responsive neurons (**Fig 2A, B**). Application of the competitive nicotinic antagonist DHBE (10 µM, 10 min) left residual acetylcholine-evoked Ca^{2+} signals in Chrna5+ neurons (35 ± 3 % of baseline, n = 71 cells, 6 mice; **Fig 2C i**) that were greater to those in Syt6+ neurons (21 ± 3% of baseline, n = 112 cells, 7 mice; Mann Whitney U = 2400, $P < 10^{-4}$). The cumulative distribution of responses remaining after DHBE was significantly right-shifted in Chrna5+ neurons compared to Syt6+ neurons (**Fig 2C ii**, Kolmogorov Smirnov D = 0.37, $P < 10^{-4}$). A majority of Chrna5+ neurons (~83%) still showed acetylcholine-evoked responses after DHBE, whereas fewer Syt6+ neurons (~50%) retained their responses, with a complete elimination of acetylcholine-evoked responses in the rest (**Fig 2C iii**, Fisher's exact test: $P < 10^{-4}$). Yet, the addition of muscarinic antagonist atropine did not attenuate the striking differences between Chrna5+ and Syt6+ neurons, raising the possibility of an underlying nicotinic mechanism (**Fig 2D**). In the presence of DHBE+ atropine, a subset of Chrna5+ neurons still showed substantial acetylcholine-evoked

Ca^{2+} signals (6 ± 1 % of baseline; **Fig 2D i**), whereas almost all Syt6+ neurons' responses were completely blocked (0.2 ± 0.1 % of baseline; Mann Whitney U = 2083, $P < 10^{-4}$) as seen from the cumulative distribution (**Fig 2D ii**, Kolmogorov Smirnov D = 0.36, $P < 10^{-4}$). The proportion of Chrna5+ and Syt6+ neurons showing acetylcholine-evoked responses after DHBE+ Atropine was significantly different (41% Chrna5+ vs 6% Syt6+, Fisher's exact test: $P < 10^{-4}$, **Fig 2D iii**). However, since DHBE is a competitive antagonist, it can be outcompeted by exogenous acetylcholine at high affinity nicotinic receptors. Therefore, we hypothesized that the resilient exogenous acetylcholine-evoked responses would require non-competitive antagonist.

To address the hypothesis of higher-affinity nicotinic binding and its consequences for spiking in these neurons, we switched to whole-cell recording in individual Chrna5+ and Syt6+ neurons. We recorded current clamp responses to acetylcholine (1 mM, 15 s) in labeled Chrna5+ and Syt6+ neurons from *Chrna5*-$Cre^{/+}$Ai14$^{/+}$ and *Syt6*-$Cre^{/+}$Ai14$^{/+}$ or *Syt6*-EGFP mice respectively (**Fig 2E**). Chrna5+ neurons showed stronger acetylcholine-evoked firing: attaining significantly higher peak firing frequency (29 ± 6 Hz, n=12 cells, 6 mice; $t_{(24)} = 2.74$, $P = 0.01$, unpaired t-test; Cohen's d: 1.08) compared to Syt6+ neurons (13 ± 2 Hz, n = 14 cells, 5 mice; **Fig 2E**). The intrinsic electrophysiological properties of Chrna5+ and Syt6+ neurons did not show statistically significant differences (**Suppl Table 2**). We next examined the sensitivity of acetylcholine-evoked firing to competitive nicotinic receptor block by DHBE in the presence of atropine. Acetylcholine-evoked firing was completely eliminated in all Syt6+ neurons (**Fig 2F**) whereas a large subset of Chrna5+ neurons (7/11) retained their ability to respond to acetylcholine (Average peak firing rate in Chrna5+ neurons: 6 ± 2 Hz; $t_{(19)} = 3.22$, $P = 0.004$, unpaired t-test) demonstrating similar resilience to competitive nicotinic receptor block as observed with Ca^{2+} imaging. We used the non-competitive nicotinic receptor blocker mecamylamine (Papke et al., 2013; Webster et al., 1999) to test our hypothesis that nicotinic receptors in this Chrna5+ subset were higher affinity and therefore allowed exogenous acetylcholine to outcompete DHBE. The addition of 5 μM mecamylamine was sufficient to eliminate acetylcholine-evoked firing in all the Chrna5+ neurons that were resilient to competitive nicotinic block ($t_{(4)} = 5.14$, $P = 0.007$, paired t-test; **Fig 2F**). Together, our Ca^{2+} imaging and electrophysiology experiments revealed the existence of a distinct subset of Chrna5+ neurons dissimilar to Syt6+ neurons, with high affinity nicotinic responses resilient to competitive nicotinic antagonism.

Single-cell transcriptomics identifies Chrna5+ subplate neurons with Lynx genes

To determine the molecular identity of distinct Chrna5+ neurons with enhanced cholinergic responses, we pursued single-cell RNAseq. We extracted gene expression data of L5-6 glutamatergic neurons (n = 2422 cells) in the mouse anterior cingulate cortex from the Allen Institute single cell RNAseq databases (Tasic et al., 2016, 2018; Yao et al., 2021). We classified these deep-layer pyramidal neurons into 3 groups: those expressing only *Chrna5* (Chrna5+, n= 243), both *Chrna5* and *Syt6* (Chrna5+ Syt6+, n = 834), or only *Syt6* (Syt6+, n = 564) **(Fig 3A)**. 781 cells showed no expression of *Chrna5* or *Syt6* and consisted primarily of L6 Intratelencephalic cells which have been previously shown to have purely muscarinic M2/M4 mediated hyperpolarizing cholinergic responses (Venkatesan and Lambe, 2020; Yang et al.,

2020). We focused on the Chrna5+, Syt6+ and Chrna5+Syt6+ groups to examine their transcriptomic differences. Single-cell analysis revealed that the Chrna5+ group primarily included L6b (44%), L5 near-projecting (L5NP, 19%), and L6CT neurons (30%), whereas the Chrna5+Syt6+ and Syt6+ groups were predominantly composed of L6CT neurons (>90%) **(Fig 3B)**. We examined the expression of marker genes in these respective groups to validate our cell-classification. Chrna5+ neurons showed distinctive expression of several marker genes- *Ctgf, Cplx3, Kcnab1, Lpar1* **(Fig 3B,C)** associated with subplate neurons (Ghezzi et al., 2021; Hoerder-Suabedissen and Molnár, 2013). Subplate neurons are early-born and vital for brain development, leaving L6b neurons as descendants in adulthood (Kanold and Luhmann, 2010; Luhmann et al., 2018; Wess et al., 2017). Notably, the highest fold enrichment among all differentially expressed genes in Chrna5+ neurons was found for subplate markers *Ctgf* (Fold change, 5.69) and *Cplx3* (3.81) (**Table 1)**. Overall, Chrna5+ neurons including both L5NP and L6b subpopulations highly express subplate marker genes. In contrast, *Syt6*-expressing Chrna5+Syt6+ and Syt6+ groups are only enriched in the corticothalamic markers *Foxp2* and *Syt6*, consistent with their corticothalamic subtype. These results support our imaging, electrophysiological, and pharmacological results suggesting the exclusive Chrna5+ population is a distinct cell type from typical L6CT *Syt6*-expressing neurons.

To identify molecular changes predictive of Chrna5+ nicotinic 'super-responders', we examined differential expression of genes that exert effects on postsynaptic cholinergic responses (**Fig 3D-E**). We selected cholinergic receptor genes (nicotinic *Chrna5-2, Chrna7, Chrnb2-4*, and muscarinic subunits *Chrm1-4*), acetylcholinesterase (*Ache*), and members of the family of genes that encode lynx proteins (*Ly6e, Ly6h, Ly6g6e, Lynx1, Lypd1, Lypd6, Lypd6b*) known to allosterically modulate nicotinic receptor responses (Miwa et al., 2019). We found substantial and highly significant changes in the expression of three lynx prototoxins *Lypd1*, *Ly6g6e* and *Lypd6b* **(Fig 3D)**. While both Chrna5+ and Chrna5+Syt6+ populations express *Chrna5*, there was slightly higher expression of *Chrna5* (25% increase) as well as lower expression of the inhibitory muscarinic receptor *Chrm2* (20% decrease) in Chrna5+Syt6+ neurons. There were no significant differences in other nicotinic and muscarinic subunit expression between the two groups. Acetylcholinesterase, the enzyme that breaks down acetylcholine was also highly expressed (50% increase) in Chrna5+ neurons, which may benefit their nicotinic responses by protecting receptors from overactivation and desensitization. The fold-change of the genes in **Fig 3E** between Chrna5+ and Chrna5+Syt6+ neurons is shown in **Suppl Table 3**. Notably, the top three genes with highest fold change in Chrna5+ neurons were the GPI-anchored lynx prototoxins: Lynx2 encoded by *Lypd1* (Fold change: 2.55), *Ly6g6e* (2.03), and *Lypd6b* (1.51). The distinct pattern of expression of specific lynx proteins in Chrna5+ neurons suggests unexpectedly complex endogenous control of nicotinic responses in these prefrontal subplate neurons.

Perturbing native prefrontal cortical lynx-modulation of optogenetic nicotinic responses

To examine whether the molecular machinery of deep layer prefrontal neurons endows them with greater dynamic range in responding to acetylcholine, we sought to experimentally perturb endogenous lynx modulation. Members of the lynx-family are GPI-anchored (**Fig 4A**), and work in cell expression systems (Wu et al., 2015) suggests these anchors can be cleaved via activation

of phospholipase C (PLC). These experiments are important because the potential impact of GPI cleavage on nicotinic responses in a native system is not well understood. We hypothesized that perturbing lynx-mediated control could affect endogenous nicotinic properties in a complex manner (**Fig 4A**) since both positive (eg. Ly6g6e) and negative modulatory lynx proteins (eg. Lynx1) are expressed. To cleave GPI-anchored proteins, we used the PLC activator compound m-3M3FBS (Bae et al., 2003; Horowitz et al., 2005; Krjukova et al., 2004; Sturgeon and Magoski, 2018). Nicotinic responses of deep layer pyramidal neurons from ChAT-ChR2 mice to optogenetic acetylcholine release were recorded in the continuous presence of atropine before and after treatment with m-3M3FBS (25μM, 5 min; **Fig 4B**). The rising slope of the nicotinic responses showed a significant increase after m-3M3FBS treatment (23 ± 17%; Paired Cohen's d = 0.83; P = 0.008, Wilcoxon matched-pairs test), compared to the baseline change observed in the same cells prior to PLC activation (-6 ± 4%; 8 cells, 6 mice; **Fig 4C, D**). This increase was not observed with the inactive ortholog o-3M3FBS that does not activate PLC (Paired Cohen's d = 0.09, P = 0.625, Wilcoxon matched-pairs test, data not shown). The area under the nicotinic response known as charge transfer also showed a statistically significant increase following PLC activation (22 ± 7%; Cohen's d = 1.68; P = 0.016, Wilcoxon matched-pairs test; **Fig 4D**), compared to baseline change (-9 ± 6%). Thus, PLC activation causes a specific increase in nicotinic receptor responses, presumably due to cleavage of inhibitory GPI-anchored prototoxins such as Lynx1.

To test the transcriptomic prediction that cell-type specific differences in lynx modulation lead to different cholinergic properties, we obtained purified water-soluble recombinant Ly6g6e protein and examined its effects on optogenetic nicotinic responses in labeled Chrna5+ and Syt6+ neurons (**Fig 4F**). These experiments were conducted in *Chrna5*-Cre$^{/+}$Ai14$^{/+}$ChAT-ChR2$^{/+}$ and *Syt6*-Cre$^{/+}$Ai14$^{/+}$ChAT-ChR2$^{/+}$ mice. We hypothesized that the modulation of Chrna5+ neuronal nicotinic receptors by endogenous Ly6g6e would occlude the effect of exogenous soluble Ly6g6e, whereas Syt6+ neurons would be altered by exposure to the exogenous Ly6g6e (Fig 4G). Consistent with this hypothesis, we found that 10 minute application of soluble Ly6g6e did not significantly alter the amplitude of optogenetically evoked nicotinic responses in labeled Chrna5+ neurons (Change in peak = -2.1 ± 1.2 pA, $t_{(6)}$ = 1.79, P = 0.12, paired t-test). However, in labeled Syt6+ neurons lacking endogenous expression of *Ly6g6e*, exogenous application of soluble Ly6g6e caused a significant decrease in the amplitude (Change in peak = -10 ± 1.8 pA, $t_{(8)}$ = 5.60, P < 0.001, paired t-test; **Fig 4H-I**). The change in peak and area of the nicotinic responses caused by solube Ly6g6e was significantly different between Chrna5+ and Syt6+ neurons (change in peak : $t_{(14)}$ = 3.43, P = 0.004; Change in area: $t_{(14)}$ = 2.53, P = 0.024, Unpaired t test; **Fig 4I - J**). Of note, soluble and endogenous GPI-anchored prototoxins are known to have opposite effects on nicotinic receptors and the exact direction of endogenous modulation of nicotinic receptors by different lynx proteins is still debated (Arvaniti et al., 2016; Kulbatskii et al., 2021; Miwa, 2021). The key outcome of this experiment is the difference in the Ly6g6e modulation of Chrna5+ and Syt6+ neurons, not the direction. We conclude that Chrna5+ neurons exert specialized molecular control over their nicotinic receptors, shaping their fate as acetylcholine super-responders.

Discussion (1206 words)

Our work examines the effects of GPI-anchored lynx prototoxins on native nicotinic receptor-mediated optogenetic responses, advancing from work in heterologous expression systems.

These results are a first step in showing how endogenous lynx regulation of nicotinic responses can act in a complex cell-type specific fashion leading to specialized cholinergic properties in a subset of neurons. Overall, our study reveals a previously uncharacterized population of *Chrna5*-expressing subplate neurons in the prefrontal cortex that are exquisitely sensitive to acetylcholine, with differential expression of several lynx prototoxin genes that allow flexible tuning of their high-affinity nicotinic responses (**Fig 5**).

Specialized cholinergic properties of Chrna5-expressing neurons

While important for attention, the neurophysiological impact of the auxiliary α5 nicotinic subunit in its native neuronal environment has remained beyond the reach of previous work. The contributions of α5 to high-affinity nicotinic receptors have been extrapolated based on results of cell system experiments and work in rodents deleted for *Chrna5* (Bailey et al., 2010; Howe et al., 2018b; Kuryatov et al., 2008; Prevost et al., 2020; Venkatesan and Lambe, 2020). Here, *Chrna5*-Cre mice allowed us to affirmatively demonstrate that neurons expressing the α5 nicotinic subunit respond faster and more strongly to endogenous acetylcholine. This cholinergic heterogeneity among layer 6 neurons prompted a larger scale comparison between Chrna5+ neurons and a well-defined layer 6 population labeled by *Syt6* (Nectow et al., 2017a). These experiments revealed a subset of Chrna5+ acetylcholine 'super-responders' with high affinity nicotinic responses that were not found in Syt6+ neurons.

Heterogeneity of cell types expressing Chrna5

Previously, the deep-layer cell types expressing *Chrna5* were uncharacterized, and generally thought to include L6CT neurons (Kassam et al., 2008). Investigation of L6CT neurons have relied on *Syt6*-Cre and *Ntsr1*-Cre mouse lines that label similar sets of neurons (Harris et al., 2014, 2019; Nectow et al., 2017a), with only *Syt*6-Cre mice successfully labeling this population in prefrontal cortex (Vaasjo et al., 2021). L6CT neurons labeled by *Syt6* or *Ntsr1* expression are excited by acetylcholine (Sundberg et al., 2018; Tian et al., 2014), but the degree to which their nicotinic response relied on *Chrna5* expression was unclear. Strikingly, we reveal that acetylcholine super-responders with high affinity nicotinic receptors are from the population of Chrna5+ neurons without *Syt6*-expression. Transcriptomic analysis demonstrates that majority of these likely Chrna5+ 'super-responders' arise from L5 Near-Projecting and L6b neurons, populations that express multiple markers linking them to the developmental subplate. These enigmatic cells are remnants of earliest-born cortical neurons that serve as a relay for establishing connections between cortex and thalamus (Marx et al., 2017; Molnár et al., 2020). Subplate neurons receive cholinergic inputs at birth (Mechawar and Descarries, 2001), highlighting their role in developmental cholinergic modulation.

Advantages of Chrna5 as a marker for subplate cells

In contrast to L6CT neurons, subplate neurons remain relatively uncharacterized due to the lack of transgenic mice to definitively label the diverse subtypes, and inaccessibility of the available lines for *in vivo* targeting. Transcriptomic analysis (Fig 5, Table 1) suggests that the Chrna5+ population is enriched for known subplate markers *Ctgf* (Connective tissue growth factor), *Cplx3* (Complexin 3), *Kcnab1,*and *Lpar1* (Hoerder-Suabedissen and Molnár, 2013; Hoerder-Suabedissen et al., 2009; Tiong et al., 2019). Significantly, the lynx prototoxin and nicotinic

receptor modulator *Ly6g6e*, which is highly expressed in Chrna5+ neurons, is also a marker of subplate neurons (Hoerder-Suabedissen et al., 2013). Our study is the first to identify enhanced cholinergic activation regulated by *Chrna5* and lynx-gene expression in subplate/L6b neurons. Subplate neurons have recently been found to strongly regulate cortical output through their intracortical connections (Egger et al., 2020; Zolnik et al., 2020). Enhanced cholinergic activation in these neurons will have different consequences for prefrontal processing, challenging the popular conception that cholinergic modulation of attention occurs only through top-down control of thalamic input by L6CT neurons.

Molecular determinants of nicotinic receptor properties in Chrna5+ neurons

Our transcriptomic analysis revealed enhanced expression of GPI-anchored lynx prototoxin genes *Ly6g6e*, *Lypd1*, and *Lypd6b* in Chrna5+ neurons (Fig 5). Lynx proteins are well known modulators of nicotinic receptor properties and trafficking (Anderson et al., 2020; Miwa, 2021), but most of the insight into their actions comes from heterologous cell systems, deletion, and overexpression experiments. Their effects on nicotinic receptors in their native environment is unclear. In expression systems, Ly6g6e potentiates α4β2 nicotinic responses, slowing their desensitization (Wu et al., 2015), predicting cholinergic responses in Chrna5+ neurons would be resistant to desensitization as has been implied by *Chrna5* deletion work (Venkatesan and Lambe, 2020). In contrast, Lynx2 (*Lypd1*) is a predicted negative modulator that can increase desensitization of α4β2 nicotinic receptors (Tekinay et al., 2009). Lynx2 acts intracellularly to reduce surface expression of α4β2 nicotinic receptors (Wu et al., 2015), but may preferentially act on lower affinity $(\alpha4)_3(\beta2)_2$ receptors (Kuryatov et al., 2008; Nichols et al., 2014) and indirectly promote expression of high affinity $(\alpha4)_2(\beta2)_2\alpha5$ nicotinic receptors. The effect of Lypd6b on $(\alpha4)_2(\beta2)_2\alpha5$ nicotinic receptors is yet to be determined and may further contribute to the complex control of Chrna5+ nicotinic responses (Ochoa et al., 2016). In addition, Lynx1, a well-known negative modulator of α4β2 nicotinic receptors (Falk et al., 2021; Ibañez-Tallon et al., 2002; Miwa et al., 1999; Morishita et al., 2010) is also expressed in Chrna5+ neurons. Consistent with such complex lynx regulation, our experiments confirmed that removing GPI-anchored lynx proteins increases nicotinic response onset and amplitude potentially due to removal of Lynx1. In contrast, exogenous application of recombinant Ly6g6e had different effects in Chrna5+ and Syt6+ neurons, consistent with cell-type specific lynx modulation in Chrna5+ neurons predicted by transcriptomics.

Functional consequences

The effects of lynx proteins on nicotinic receptor function have so far been determined by heterologous expression systems (Wu et al., 2015), knockout studies (Sherafat et al., 2021; Tekinay et al., 2009), exogenous application of recombinant water-soluble lynx proteins (Shenkarev et al., 2020; Thomsen et al., 2016), and viral manipulation of expression in the brain (Falk et al., 2021; Sadahiro et al., 2020). We advance this field by revealing, in native tissue, complex endogenous regulation of optogenetic nicotinic responses by multiple GPI-anchored lynx proteins. Inhibitory lynx expression and high levels of acetylcholinesterase in Chrna5+ neurons suggest that their responses are restrained and our experiments likely underestimated their nicotinic receptor function. These responses could be dramatically enhanced when

acetylcholinesterase and inhibitory lynx modulation is reduced through other signaling mechanisms. Such flexible tuning of nicotinic responses by lynx prototoxins in Chrna5+ neurons can provide greater dynamic range and poises them to be key players during attentional processing (Fig 5). A recent study found that preventing developmental increase in Lynx1 expression in corticocortical neurons by viral knockdown led to altered cortical connectivity and impaired attention (Falk et al., 2021). Thus cell-type specific changes in lynx expression during development are critical for maturation of attention circuits. It is of interest to examine such changes during development in Chrna5+ neurons and how they differ from Syt6+ neurons.

Summary of advances

Our study reveals a distinct group of 'acetylcholine super-responder' neurons in the prefrontal cortex identified by *Chrna5*-expression that constitute subplate neurons vital for cortical development. We identify that their high affinity α5 subunit-containing nicotinic receptors are under complex regulation by several lynx prototoxins and acetylcholinesterase. *Chrna5*-Cre mice are a valuable tool for future studies examining the in vivo role of these specialized neurons.

Acknowledgements: We acknowledge the generous support of the Canadian Institutes of Health Research (CIHR MOP 89825, EKL; CIHR PJT-153101, EKL), the Canada Research Chair in Developmental Cortical Physiology (EKL), an Ontario Graduate Scholarship (SV). We thank Ms. Janice McNabb and Mr. Ha-Seul Jeoung for expert technical assistance. Earlier presentations of this work received valuable feedback from Dr. Junchul Kim, Dr. Beverly Orser, and Dr. Steve Prescott of the University of Toronto.

Conflicts of interest: None

Figure legends

Figure 1. *Chrna5* expression identifies a distinct population of prefrontal neurons with stronger and faster-onset optogenetic cholinergic responses. A, Breeding scheme to obtain triple transgenic *Chrna5*-Cre$^{/+}$Ai14$^{/+}$ChAT-ChR2$^{/+}$ mice expressing tdTomato in *Chrna5*-expressing (Chrna5+) neurons and Channelrhodopsin 2 in cholinergic axons. **B,** (*Top*) Schematic of coronal mPFC slice with region of interest, adapted from (Paxinos and Franklin, 2004). (*Bottom*) two photon imaging (3D projection) of tdTomato-labeled Chrna5+ neurons and EYFP-labeled cholinergic axons in layer 6 of mPFC slices. **C,** IRDIC (*left*) and widefield fluorescence (TRITC, *right*) images of tdTomato labeled Chrna5+ and unlabeled layer 6 neurons during whole cell patch clamp electrophysiology. Clearing induced by the pipette is visible. **D,** Average light-evoked endogenous cholinergic response of labeled Chrna5+ vs neighbouring unlabeled Chrna5- neurons. Dotted lines are the slope of the response onset. (*Inset*) Individual responses are zoomed in to show the onset. **E-F,** Bar graph comparing (E) Rising slope and (F) Peak current of endogenous cholinergic responses between labeled Chrna5+ neurons (n = 24 cells) and unlabeled Chrna5- neurons (n = 15 cells, 4 mice). *$P < 0.05$, Unpaired t-test. **G,** (*Top*) Breeding scheme to obtain triple transgenic *Chrna5*-Cre$^{/+}$Ai14$^{/+}$*Syt6*-EGFP$^{/+}$ mice expressing tdTomato in Chrna5+ neurons and EGFP in Syt6+ neurons. (*Bottom*) Confocal imaging in mPFC slices shows Chrna5+ and Syt6+ neurons distributed in layer 6. **H-I,** Confocal (H) and two-photon imaging (I) reveal three populations of neurons: exclusively Chrna5+ neurons which do not express *Syt6*, overlapping Chrna5+Syt6+ neurons which express both markers, and exclusively Syt6+ neurons which do not express *Chrna5*. **J,** (*left*) Graph quantifies the percentage of each cell type with respect to all labeled cells per sample. (*Right*) Average proportions of Chrna5+, Chrna5+Syt6+ and Syt6+ neurons.

Figure 2. Calcium imaging in Chrna5+ and Syt6+ populations reveals a distinct subset of Chrna5+ neurons with resilient nicotinic responses. A, (*Top*) Two photon Ca^{2+} imaging in prefrontal brain slices from *Chrna5*-Cre$^{/+}$Ai96$^{/+}$ (*left*) and *Syt6*-Cre$^{/+}$Ai96$^{/+}$ mice (*right*) showing acetylcholine-evoked GCaMP6s responses in Chrna5+ and Syt6+ neurons respectively (scale 50 μm). (*Bottom*) Acetylcholine-evoked GCaMP6s signals were sequentially recorded after application of competitive nicotinic antagonist DHBE and addition of muscarinic antagonist atropine (scale 10 μm). **B,** Normalized fluorescence signal **(**ΔF by F) evoked by acetylcholine in individual Chrna5+ and Syt6+ neurons in a brain slice at baseline (*left*), after DHBE (*middle*), and after DHBE + Atropine (*right*). (Inset, average response and standard deviation. Scale: same as main figure). **C-D i,** Boxplot shows the percentage of response remaining after the application

of (C) DHBE and (D) DHBE + Atropine (Inset shows the same boxplot with a restricted y-axis, '+' symbols denote respective means). Responses were quantified by the area under the ΔF/F curve (n = 71 neurons, 6 mice for Chrna5+, and 112 neurons, 7 mice for Syt6+, ****$P < 10^{-4}$, Mann-Whitney test). **C-D ii,** Cumulative frequency distribution of the percentage response remaining after **(**C) DHBE and (D) DHBE + Atropine ($P < 10^{-4}$, Kolmogorov-Smirnov test). **C-D iii,** Proportion of cells showing zero and non-zero responses after (C) DHBE and (D) DHBE + Atropine ($P < 10^{-4}$ for both C & D, Fisher's exact test). **E,** Current clamp responses evoked by 1mM acetylcholine (15s) in fluorescently labeled Chrna5+ and Syt6+ layer 6 neurons patched in mPFC slices from mice *Chrna5*-Cre$^{/+}$ Ai14$^{/+}$ and *Syt6*-Cre$^{/+}$Ai14$^{/+}$ or *Syt6*-EGFP mice respectively. **F,** Peak spike frequency in Chrna5+ and Syt6+ neurons evoked by acetylcholine (*left*), and in the presence of competitive nicotinic antagonist DHBE and atropine (*middle;* **$P < 0.01$,*$P < 0.05$, unpaired t-test). Residual response remaining after DHBE + Atropine in Chrna5+ neurons is blocked by non-competitive nicotinic antagonist mecamylamine (*right*, **$P < 0.01$, paired t-test).

Figure 3. Single cell transcriptomic analysis reveals Chrna5+ subset to span subplate neuron populations with differential expression of lynx prototoxin genes A, Single cell-RNAseq data for 2422 L5-6 glutamatergic neurons in the anterior cingulate cortex (ACA, shown in schematic on the left) was obtained from publicly available datasets (Allen Institute, SMARTSeq ACA and MOP (2018)). (*Right*) Scatter plot showing *Chrna5* vs *Syt6* expression in $\log_{10}$ (Copies per million +1) for each neuron, with the frequency distribution shown on the corresponding axes. Neurons were classified into Chrna5+, Chrna5+Syt6+ and Syt6+ groups based on their expression of *Chrna5* and *Syt6* genes. Cells which expressed neither gene were excluded from subsequent analyses. **B**, The major neuronal subclasses within Chrna5+, Chrna5+Syt6+ and Syt6+ groups is indicated by the colorbar on top. NP- Near projecting, CT-Corticothalamic. Heatmap shows expression of subplate and corticothalamic marker genes in each cell in all 3 groups. **C,** Dotplot shows summary of subplate and corticothalamic marker expression in Chrna5+, Chrna5+Syt6+ and Syt6+ groups. Dot size indicates the percentage of cells within each group expressing that gene, color of the dot indicates average expression level relative to other groups. Chrna5+ neurons highly express multiple subplate marker genes, but not corticothalamic markers. **D**, Violin plots show expression of Lynx prototoxin genes *Ly6g6e*, *Lypd1* (Lynx2) and *Lypd6b* which show highest fold-change between Chrna5+ and Chrna5+Syt6+ neurons. **E,** Dotplot shows expression of major genes known to modulate cholinergic function, including nicotinic, muscarinic subunits, acetylcholinesterase, and lynx prototoxins in Chrna5+, Chrna5+Syt6+ and Syt6+ neurons. Genes are ordered by decreasing fold change in expression. Dot size indicates the percentage of cells within each group expressing that gene, color of the dot indicates average expression level relative to other groups. Fold change of all the genes shown in this dotplot are listed in Supplemetary table 3.

Figure 4. Regulation of optogenetic nicotinic responses by endogenous GPI-anchored lynx proteins and cell type specific effects of recombinant Ly6g6e. A, Schematic of nicotinic receptor environment showing endogenous GPI-anchored lynx proteins exerting positive and negative modulation of nicotinic receptors. The compound m-3M3FBS activates PLC, cleaving the GPI anchor and perturbing lynx-mediated modulation of nicotinic responses. **B,** Optogenetic

nicotinic responses in prefrontal deep-layer pyramidal neurons from ChAT-ChR2 mice before and after treatment with m-3M3FBS (5 min). **C,** PLC activation significantly increased the rising slope of optogenetic nicotinic responses. Percent change in **D,** Rising slope and **E,** Area of nicotinic response in control and after PLC activation. (**P* < 0.05, ***P* < 0.01, Wilcoxon matched-pairs test). **F,** IRDIC (*left*) and widefield fluorescence (*right*) images of tdTomato labeled Chrna5+ (*top*) and Syt6+ (*bottom*) neurons during whole-cell patch clamp electrophysiology in *Chrna5*-Cre$^{/+}$Ai14$^{/+}$ChAT-ChR2$^{/+}$ and *Syt6*-Cre$^{/+}$Ai14$^{/+}$ChAT-ChR2$^{/+}$ mouse brain slices respectively. **G,** Schematic summarising predicted and observed effects of recombinant water-soluble ly6g6e on Chrna5+ and Syt6+ neuronal nicotinic receptors. **G,** Optogenetic nicotinic responses are reduced in amplitude following 10 minute application of soluble ly6g6e in Syt6+ but not Chrna5+ neurons. Change in peak current (**I**) and area of the nicotinic response (**J**) of Chrna5+ vs Syt6+ neurons (**P* < 0.05, ** *P* < 0.01, Unpaired t-test)

Figure 5. Graphical summary. Deep-layer pyramidal neurons can be divided into three groups (Chrna5+, Chrna5+Syt6+, Syt6+) by their expression of *Chrna5* and *Syt6* genes. The subset of *Chrna5*-expressing neurons without *Syt6* expression are molecularly distinct and comprise of subplate neurons, whereas *Syt6*-expressing neurons are of the corticothalamic subtype. Nicotinic receptors in these neurons are under complex regulation by endogenous lynx prototoxins. Inhibitory prototoxin gene *Lynx1* is expressed uniformly in all neurons, whereas Chrna5+ subplate neurons additionally have specific expression of *Ly6g6e*, *Lypd1* and *Lypd6b* prototoxin genes. These Chrna5+ subplate neurons show enhanced α5 subunit nicotinic receptor-mediated cholinergic responses that are differently modulated by specific lynx prototoxins.

STAR Methods

Experimental model and subject details

Syt6-Cre$^{/+}$GCaMP6s$^{/+}$ and *Chrna5*-Cre$^{/+}$GCaMP6s$^{/+}$ mice used for Ca^{2+} imaging were obtained by crossing *Chrna5*-Cre (Gift from Dr. Eric Turner) and *Syt6*-Cre mice (*Syt6*-Cre KI148, RRID:MMRRC 037416-UCD, (Gong et al., 2007)) respectively, with Ai96 mice (JAX: 024106). For electrophysiological recordings of labeled Chrna5+ and Syt6+ neurons, we used *Chrna5*-Cre$^{/+}$Ai14$^{/+}$, and *Syt6*-Cre$^{/+}$Ai14$^{/+}$ mice respectively. *Syt6*-EGFP$^{/+}$ mice were additionally used for few experiments (*Syt6*-EGFP EL71, RRID:MMRRC 010557-UCD, (Gong et al., 2003)).

Triple transgenic mice labeling both *Chrna5* and *Syt6*-expressing neurons with EGFP in Syt6+ neurons and tdTomato in Chrna5+ neurons were used to examine the overlap between the two cell types. *Syt6*-EGFP and Ai14 mice (Madisen et al., 2010) were bred together and the offspring were crossed with *Chrna5*-Cre mice to generate *Chrna5*-Cre$^{/+}$Ai14$^{/+}$*Syt6*-EGFP$^{/+}$ mice used for these experiments. A set of experiments measuring optogenetic cholinergic responses was also performed in ChAT-ChR2 (ChAT$^{/+}$) mice (JAX: 014546). To examine optogenetic cholinergic responses in labeled Chrna5 and Syt6 cell populations, the respective Cre lines were crossed with ChAT$^{/+}$Ai14$^{/+}$ mice to generate *Chrna5*-Cre$^{/+}$Ai14$^{/+}$ChAT$^{/+}$ and *Syt6*-Cre$^{/+}$Ai14$^{/+}$ChAT$^{/+}$ mice.

All animals were bred on a C57BL/6 background, except *Syt6*-EGFP which were Black Swiss. Adult male and female animals age >P60 were used in the study. Mice were separated based on sex after weaning at P21 and group-housed (2-4 mice per cage). Animals had ad libitum access to food and water and were on a 12-h light/dark cycle with lights on at 7 AM. Guidelines of the Canadian Council on Animal Care were followed, and all experimental procedures were approved by the Faculty of Medicine Animal Care Committee at the University of Toronto. 42 mice were used for the entire study, with similar numbers of males and females.

Method details

Brain slicing and electrophysiology

Slicing and electrophysiology followed procedures described previously (Venkatesan and Lambe, 2020). An intraperitoneal injection of chloral hydrate (400 mg/kg) was given to anesthetize mice prior to decapitation. The brain was rapidly extracted in ice cold sucrose ACSF (254 mM sucrose, 10 mM D-glucose, 26 mM $NaHCO_3$, 2 mM $CaCl_2$, 2 mM $MgSO_4$, 3 mM KCl and 1.25 mM NaH_2PO_4). 400 μm thick coronal slices of prefrontal cortex (Bregma 2.2 - 1.1) were obtained on a Dosaka linear slicer (SciMedia, Costa Mesa, CA, USA). Slices were left to recover for at least 2 hours in oxygenated (95% O_2, 5% CO_2) ACSF (128 mM NaCl, 10 mM D-glucose, 26 Mm $NaHCO_3$, 2 mM $CaCl_2$, 2 mM $MgSO_4$, 3 Mm KCl, and 1.25 mM NaH_2PO_4) at 30°C before being used for electrophysiology or two-photon Ca^{2+} imaging. Brain slices were transferred to the stage of a BX51WI microscope (Olympus, Tokyo, Japan) and perfused with

oxygenated ACSF at 30°C. Recording electrodes (2 - 4 MΩ) containing patch solution (120 mM potassium gluconate, 5 mM KCl, 10 mM HEPES, 2 mM $MgCl_2$, 4 mM K_2-ATP, 0.4 mM Na_2-GTP and 10 mM sodium phosphocreatine, pH adjusted to 7.3 using KOH) were used to patch pyramidal neurons in layer 6 - 6b based on morphology and proximity to white matter. Only regular spiking neurons were included. Multiclamp 700B amplifier at 20 kHz with Digidata 1440A and pClamp 10.7 software (Molecular devices) were used for data acquisition. All recordings were compensated for liquid junction potential (14 mV). Voltage-clamp responses were examined at -75 mV and in current-clamp at rest or starting from -70 mV.

Optogenetics

5 ms pulses of blue light (473 nm) were delivered through the 60X objective lens with an LED (Thorlabs, 2 mW) to excite channelrhodopsin containing cholinergic fibers. Pattern of stimulation was as in a previous study, with 8 pulses of light delivered in a frequency accommodating manner (Venkatesan and Lambe, 2020).

Pharmacology

Acetylcholine (1mM, Sigma) was used to exogenously stimulate cholinergic receptors. Atropine (200 nM, Sigma) and Dihydro-β-erythroidine (DHBE, 10 μM, Tocris) were used to competitively block muscarinic receptors and β2 subunit-containing nicotinic receptors respectively. Mecamylamine (5 μM, Tocris) was used to further non-competitively block nicotinic receptors. Phospholipase C activator m-3M3FBS (25 μM, Tocris) was used to cleave GPI-anchored Lynx prototoxins and the inactive ortholog o-3M3FBS (25 μM, Tocris) was used as a control (Bae et al., 2003). Cyclodextrin (1 mM, Tocris) was included in a small subset of experiments to improve solubility of 3M3FBS compounds, but no further improvement in efficacy was observed. Water soluble recombinant Ly6g6e (0.5 mg/ml) was obtained by custom purification (Creative Biomart) and used for exogenous application at 1: 1000 and 3:1000 dilution. Effects on nicotinic receptors were not distinguishable between the two different protein concentrations. Only freshly thawed protein aliquots were used for experiments.

Two-photon imaging

Two-photon imaging of GCaMP6s Ca^{2+} signals in L6 neurons was performed using a 60× water-immersion objective with 0.90 numerical aperture using an Olympus Fluoview FV1000 microscope and a Titanium-Sapphire laser sapphire laser (Newport) at 930nm. Images were sampled at 512 x 512 pixels (2.4 pixels/μm) at a frame rate of 0.9 Hz. Following a 2-minute washout period for this initial application, GCaMP6s Ca^{2+} signals were measured in response to acetylcholine (1 mM, 15 s). The cellular responses to acetylcholine were measured at baseline, then after application of competitive nicotinic receptor antagonist DHBE (10 μM, 10 min), and again after the addition of muscarinic antagonist atropine (200 nM, 10 min).

Dual color two-photon imaging (910 nm excitation, using 570 nm dichroic mirror with green (540-595 nm) and red (570-620 nm) filters) was performed in brain slices of triple transgenic *Chrna5*-$Cre^{/+}$Ai14$^{/+}$*Syt6*-$EGFP^{/+}$ mice to examine overlap in fluorescent reporter expression between Chrna5+ and Syt6+ neurons. Z-stacks of 30 frames acquired in 1-μm steps were taken in layer 6 of mPFC slices and the maximum projection used to count cells with the

cell counter feature in Fiji. A set of mPFC brain slices from *Chrna5*-Cre$^{/+}$Ai14$^{/+}$*Syt6*-EGFP$^{/+}$ mice were also fixed and mounted for confocal imaging with LSM880 (Leica) microscope.

Single cell RNAseq analysis

Single cell RNAseq data for Anterior Cingulate Cortex (ACA) of adult mice was taken from the ACA and MOP Smart-Seq (2018) database, with cell-type annotations from Whole cortex & Hippocampus Smart-Seq (2019) database from the Allen Institute for Brain Science at https://portal.brain-map.org/atlases-and-data/rnaseq (Tasic et al., 2018; Yao et al., 2021). Single cell analysis was performed using the R package Seurat (v 4.04). Layer 5 and 6 glutamatergic neurons were selected and sorted into three cell classes based on their expression of *Chrna5* and *Syt6* genes: those expressing only *Chrna5* (Chrna5+, n = 243), only *Syt6* (Syt6+, n = 834), or both *Chrna5* and *Syt6* (Chrna5+Syt6+, n = 564). Expression (copies per million) greater than zero was used as the threshold. 781 cells did not express either *Chrna5* or *Syt6* and were not used in subsequent analyses. Rare cell types with fewer than 10 cells per group are not shown in the heatmap in figure 5 but are included for the differential expression analysis. The FindMarkers function in Seurat was used to identify genes differentially expressed between the Chrna5+ and Chrna5+Syt6+ populations. Adjusted p value < 0.05 was used as the cutoff for identifying differentialy expressed genes.

Quantification and Statistical Analysis

Analysis of electrophysiological data was conducted on Clampfit 10.7 and Axograph. Rising slope was measured by fitting a line to the first 50ms of the optogenetic cholinergic responses. Cholinergic response magnitude in voltage clamp was determined by peak current (picoamperes) and charge transfer (picocoulombs) measured by the area under the current response for 1 second.

GCaMP6s imaging data were extracted using the multi-measure feature in Fiji. Maximum projections across time for each experiment were first used to identify acetylcholine-responsive cells and add them to the ROI manager, then fluorescence intensity at all timepoints for each cell was measured. Fluorescence was normalized to the background fluorescence averaged over the first 10 frames. Area under the peak (AUP) of the signal after baseline correction was used to quantify the magnitude of cells' response to acetylcholine. Percentage response remaining after DHBE and DHBE+Atropine was calculated from the cell's AUP before and after the blockers.

GraphPad Prism 8 was used for statistical analysis and plotting graphs. Bar graphs depicting mean with standard error and boxplots with median and quartiles are shown. Effect sizes are reported as Cohen's d for major results (Ho et al., 2019). Unpaired t-tests or Mann-Whitney tests were used when comparing response properties between cell types, and paired t-test or Wilcoxon test to quantify effect of pharmacological manipulations within cells. Kolmogorov-Smirnov and Fisher's exact tests were used to compare cumulative distributions and proportions of cells respectively.

606 **References**

607 Ables, J.L., Görlich, A., Antolin-Fontes, B., Wang, C., Lipford, S.M., Riad, M.H., Ren, J., Hu, F., Luo,
608 M., Kenny, P.J., et al. (2017). Retrograde inhibition by a specific subset of interpeduncular α5 nicotinic
609 neurons regulates nicotine preference. Proc Natl Acad Sci U S A *114*, 13012–13017.
610 https://doi.org/10.1073/pnas.1717506114.

611 Anderson, K.R., Hoffman, K.M., and Miwa, J.M. (2020). Modulation of cholinergic activity through lynx
612 prototoxins: Implications for cognition and anxiety regulation. Neuropharmacology *174*, 108071.
613 https://doi.org/10.1016/j.neuropharm.2020.108071.

614 Arvaniti, M., Jensen, M.M., Soni, N., Wang, H., Klein, A.B., Thiriet, N., Pinborg, L.H., Muldoon, P.P.,
615 Wienecke, J., Damaj, M.I., et al. (2016). Functional interaction between Lypd6 and nicotinic
616 acetylcholine receptors. Journal of Neurochemistry *138*, 806–820. https://doi.org/10.1111/JNC.13718.

617 Bae, Y.S., Lee, T.G., Park, J.C., Hur, J.H., Kim, Y., Heo, K., Kwak, J.Y., Suh, P.G., and Ryu, S.H.
618 (2003). Identification of a Compound That Directly Stimulates Phospholipase C Activity. Molecular
619 Pharmacology *63*, 1043–1050. https://doi.org/10.1124/MOL.63.5.1043.

620 Bailey, C.D.C., De Biasi, M., Fletcher, P.J., and Lambe, E.K. (2010). The nicotinic acetylcholine receptor
621 alpha5 subunit plays a key role in attention circuitry and accuracy. J Neurosci *30*, 9241–9252.
622 https://doi.org/10.1523/JNEUROSCI.2258-10.2010.

623 Bierut, L.J., Stitzel, J.A., Wang, J.C., Hinrichs, A.L., Grucza, R.A., Xuei, X., Saccone, N.L., Saccone,
624 S.F., Bertelsen, S., Fox, L., et al. (2008). Variants in the Nicotinic Receptors Alter the Risk for Nicotine
625 Dependence. Am J Psychiatry *165*, 1163. https://doi.org/10.1176/APPI.AJP.2008.07111711.

626 Briggs, F. (2010). Organizing principles of cortical layer 6. Front Neural Circuits *4*, 3.
627 https://doi.org/10.3389/neuro.04.003.2010.

628 Briggs, F., and Usrey, W.M. (2008). Emerging views of corticothalamic function. Current Opinion in
629 Neurobiology *18*, 403–407. https://doi.org/10.1016/j.conb.2008.09.002.

630 Dalley, J.W., Cardinal, R.N., and Robbins, T.W. (2004a). Prefrontal executive and cognitive functions in
631 rodents: neural and neurochemical substrates. Neuroscience & Biobehavioral Reviews *28*, 771–784.
632 https://doi.org/10.1016/j.neubiorev.2004.09.006.

633 Dalley, J.W., Theobald, D.E., Bouger, P., Chudasama, Y., Cardinal, R.N., and Robbins, T.W. (2004b).
634 Cortical Cholinergic Function and Deficits in Visual Attentional Performance in Rats Following 192 IgG-
635 Saporin-induced Lesions of the Medial Prefrontal Cortex. Cerebral Cortex *14*, 922–932.
636 https://doi.org/10.1093/cercor/bhh052.

637 Demars, M.P., and Morishita, H. (2014). Cortical parvalbumin and somatostatin GABA neurons express
638 distinct endogenous modulators of nicotinic acetylcholine receptors. Molecular Brain *7*, 75.
639 https://doi.org/10.1186/s13041-014-0075-9.

Egger, R., Narayanan, R.T., Guest, J.M., Bast, A., Udvary, D., Messore, L.F., Das, S., de Kock, C.P.J., and Oberlaender, M. (2020). Cortical Output Is Gated by Horizontally Projecting Neurons in the Deep Layers. Neuron *105*, 122-137.e8. https://doi.org/10.1016/J.NEURON.2019.10.011.

Falk, E.N., Norman, K.J., Garkun, Y., Demars, M.P., Im, S., Taccheri, G., Short, J., Caro, K., Mccraney, S.E., Cho, C., et al. (2021). Nicotinic regulation of local and long-range input balance drives top-down attentional circuit maturation. Sci. Adv *7*. .

Ghezzi, F., Marques-Smith, A., Anastasiades, P.G., Lyngholm, D., Vagnoni, C., Rowett, A., Parameswaran, G., Hoerder-Suabedissen, A., Nakagawa, Y., Molnar, Z., et al. (2021). Non-canonical role for lpar1-egfp subplate neurons in early postnatal mouse somatosensory cortex. Elife *10*. https://doi.org/10.7554/ELIFE.60810.

Gong, S., Zheng, C., Doughty, M.L., Losos, K., Didkovsky, N., Schambra, U.B., Nowak, N.J., Joyner, A., Leblanc, G., Hatten, M.E., et al. (2003). A gene expression atlas of the central nervous system based on bacterial artificial chromosomes. Nature *425*, 917–925. https://doi.org/10.1038/NATURE02033.

Gong, S., Doughty, M., Harbaugh, C.R., Cummins, A., Hatten, M.E., Heintz, N., and Gerfen, C.R. (2007). Targeting Cre recombinase to specific neuron populations with bacterial artificial chromosome constructs. Journal of Neuroscience *27*, 9817–9823. https://doi.org/10.1523/JNEUROSCI.2707-07.2007.

Gritton, H.J., Howe, W.M., Mallory, C.S., Hetrick, V.L., Berke, J.D., and Sarter, M. (2016). Cortical cholinergic signaling controls the detection of cues. Proc Natl Acad Sci U S A *113*, E1089-97. https://doi.org/10.1073/pnas.1516134113.

Han, W., Zhang, T., Ni, T., Zhu, L., Liu, D., Chen, G., Lin, H., Chen, T., and Guan, F. (2019). Relationship of common variants in CHRNA5 with early-onset schizophrenia and executive function. Schizophrenia Research *206*, 407–412. https://doi.org/10.1016/j.schres.2018.10.011.

Harris, J.A., Hirokawa, K.E., Sorensen, S.A., Gu, H., Mills, M., Ng, L.L., Bohn, P., Mortrud, M., Ouellette, B., Kidney, J., et al. (2014). Anatomical characterization of Cre driver mice for neural circuit mapping and manipulation. Frontiers in Neural Circuits *8*, 76. https://doi.org/10.3389/fncir.2014.00076.

Harris, J.A., Mihalas, S., Hirokawa, K.E., Whitesell, J.D., Choi, H., Bernard, A., Bohn, P., Caldejon, S., Casal, L., Cho, A., et al. (2019). Hierarchical organization of cortical and thalamic connectivity. Nature *575*, 195–202. https://doi.org/10.1038/s41586-019-1716-z.

Heath, C.J., King, S.L., Gotti, C., Marks, M.J., and Picciotto, M.R. (2010). Cortico-Thalamic Connectivity is Vulnerable to Nicotine Exposure During Early Postnatal Development through α4/β2/α5 Nicotinic Acetylcholine Receptors. Neuropsychopharmacology *35*, 2324–2338. https://doi.org/10.1038/npp.2010.130.

Ho, J., Tumkaya, T., Aryal, S., Choi, H., and Claridge-Chang, A. (2019). Moving beyond P values: data analysis with estimation graphics. Nature Methods *16*, 565–566. https://doi.org/10.1038/s41592-019-0470-3.

Hoerder-Suabedissen, A., and Molnár, Z. (2013). Molecular Diversity of Early-Born Subplate Neurons. Cerebral Cortex *23*, 1473–1483. https://doi.org/10.1093/CERCOR/BHS137.

Hoerder-Suabedissen, A., Wang, W.Z., Lee, S., Davies, K.E., Goffinet, A.M., Rakić, S., Parnavelas, J., Reim, K., Nicolić, M., Paulsen, O., et al. (2009). Novel Markers Reveal Subpopulations of Subplate

679 Neurons in the Murine Cerebral Cortex. Cerebral Cortex *19*, 1738–1750.
680 https://doi.org/10.1093/CERCOR/BHN195.

681 Hoerder-Suabedissen, A., Oeschger, F.M., Krishnan, M.L., Belgard, T.G., Wang, W.Z., Lee, S., Webber,
682 C., Petretto, E., Edwards, A.D., and Molnár, Z. (2013). Expression profiling of mouse subplate reveals a
683 dynamic gene network and disease association with autism and schizophrenia. Proc Natl Acad Sci U S A
684 *110*, 3555–3560. https://doi.org/10.1073/PNAS.1218510110/SUPPL_FILE/SD02.XLSX.

685 Horowitz, L.F., Hirdes, W., Suh, B.-C., Hilgemann, D.W., Mackie, K., and Hille, B. (2005).
686 Phospholipase C in Living Cells Activation, Inhibition, Ca2+ Requirement, and Regulation of M Current.
687 Journal of General Physiology *126*, 243–262. https://doi.org/10.1085/JGP.200509309.

688 Howe, W.M., Brooks, J.L., Tierney, P.L., Pang, J., Rossi, A., Young, D., Dlugolenski, K., Guillmette, E.,
689 Roy, M., Hales, K., et al. (2018a). α5 nAChR modulation of the prefrontal cortex makes attention
690 resilient. Brain Structure and Function *223*, 1035–1047. https://doi.org/10.1007/s00429-017-1601-1.

691 Howe, W.M., Brooks, J.L., Tierney, P.L., Pang, J., Rossi, A., Young, D., Dlugolenski, K., Guillmette, E.,
692 Roy, M., Hales, K., et al. (2018b). α5 nAChR modulation of the prefrontal cortex makes attention
693 resilient. Brain Structure and Function *223*, 1035–1047. https://doi.org/10.1007/s00429-017-1601-1.

694 Ibañez-Tallon, I., Miwa, J.M., Wang, H.L., Adams, N.C., Crabtree, G.W., Sine, S.M., and Heintz, N.
695 (2002). Novel modulation of neuronal nicotinic acetylcholine receptors by association with the
696 endogenous prototoxin lynx1. Neuron *33*, 893–903. https://doi.org/10.1016/S0896-6273(02)00632-3.

697 Kanold, P.O., and Luhmann, H.J. (2010). The Subplate and Early Cortical Circuits.
698 Http://Dx.Doi.Org/10.1146/Annurev-Neuro-060909-153244 *33*, 23–48.
699 https://doi.org/10.1146/ANNUREV-NEURO-060909-153244.

700 Kassam, S.M., Herman, P.M., Goodfellow, N.M., Alves, N.C., and Lambe, E.K. (2008). Developmental
701 excitation of corticothalamic neurons by nicotinic acetylcholine receptors. J Neurosci *28*, 8756–8764.
702 https://doi.org/10.1523/JNEUROSCI.2645-08.2008.

703 Krjukova, J., Holmqvist, T., Danis, A.S., Åkerman, K.E.O., and Kukkonen, J.P. (2004). Phospholipase C
704 activator m-3M3FBS affects Ca2+ homeostasis independently of phospholipase C activation. British
705 Journal of Pharmacology *143*, 3–7. https://doi.org/10.1038/SJ.BJP.0705911.

706 Kulbatskii, D., Shenkarev, Z., Bychkov, M., Loktyushov, E., Shulepko, M., Koshelev, S., Povarov, I.,
707 Popov, A., Peigneur, S., Chugunov, A., et al. (2021). Human Three-Finger Protein Lypd6 Is a Negative
708 Modulator of the Cholinergic System in the Brain. Frontiers in Cell and Developmental Biology *9*, 2593.
709 https://doi.org/10.3389/FCELL.2021.662227/BIBTEX.

710 Kuryatov, A., Onksen, J., and Lindstrom, J. (2008). Roles of accessory subunits in α4β2* nicotinic
711 receptors. Molecular Pharmacology https://doi.org/10.1124/mol.108.046789.

712 Luhmann, H.J., Kirischuk, S., and Kilb, W. (2018). The superior function of the subplate in early
713 neocortical development. Frontiers in Neuroanatomy *12*, 97.
714 https://doi.org/10.3389/FNANA.2018.00097/BIBTEX.

715 Madisen, L., Zwingman, T.A., Sunkin, S.M., Wook Oh, S., Zariwala, H.A., Gu, H., Ng, L.L., Palmiter,
716 R.D., Hawrylycz, M.J., Jones, A.R., et al. (2010). A robust and high-throughput Cre reporting and
717 characterization system for the whole mouse brain. https://doi.org/10.1038/nn.2467.

718 Marx, M., Qi, G., Hanganu-Opatz, I.L., Kilb, W., Luhmann, H.J., and Feldmeyer, D. (2017). Neocortical
719 Layer 6B as a Remnant of the Subplate - A Morphological Comparison. Cerebral Cortex *27*, 1011–1026.
720 https://doi.org/10.1093/CERCOR/BHV279.

721 Maskos, U. (2020). The nicotinic receptor alpha5 coding polymorphism rs16969968 as a major target in
722 disease: Functional dissection and remaining challenges. Journal of Neurochemistry *154*, 241–250.
723 https://doi.org/10.1111/JNC.14989.

724 McGaughy, J., Dalley, J.W., Morrison, C.H., Everitt, B.J., Robbins, T.W., and Robbins, TW. (2002).
725 Selective behavioral and neurochemical effects of cholinergic lesions produced by intrabasalis infusions
726 of 192 IgG-saporin on attentional performance in a five-choice serial reaction time task. J Neurosci *22*,
727 1905–1913. https://doi.org/10.1523/jneurosci.5112-07.2008.

728 Mechawar, N., and Descarries, L. (2001). The cholinergic innervation develops early and rapidly in the
729 rat cerebral cortex: a quantitative immunocytochemical study. Neuroscience *108*, 555–567.
730 https://doi.org/10.1016/S0306-4522(01)00389-X.

731 Miwa, J.M. (2021). Lynx1 prototoxins: critical accessory proteins of neuronal nicotinic acetylcholine
732 receptors. Current Opinion in Pharmacology *56*, 46–51. https://doi.org/10.1016/J.COPH.2020.09.016.

733 Miwa, J.M., Ibañez-Tallon, I., Crabtree, G.W., Sánchez, R., Šali, A., Role, L.W., and Heintz, N. (1999).
734 lynx1, an Endogenous Toxin-like Modulator of Nicotinic Acetylcholine Receptors in the Mammalian
735 CNS. Neuron *23*, 105–114. https://doi.org/10.1016/S0896-6273(00)80757-6.

736 Miwa, J.M., Anderson, K.R., and Hoffman, K.M. (2019). Lynx Prototoxins: Roles of Endogenous
737 Mammalian Neurotoxin-Like Proteins in Modulating Nicotinic Acetylcholine Receptor Function to
738 Influence Complex Biological Processes. Frontiers in Pharmacology *10*, 343.
739 https://doi.org/10.3389/fphar.2019.00343.

740 Molnár, Z., Luhmann, H.J., and Kanold, P.O. (2020). Transient cortical circuits match spontaneous and
741 sensory-driven activity during development. Science *370*. https://doi.org/10.1126/science.abb2153.

742 Morishita, H., Miwa, J.M., Heintz, N., and Hensch, T.K. (2010). Lynx1, a Cholinergic Brake, Limits
743 Plasticity in Adult Visual Cortex. Science (1979) *330*, 1238–1240.
744 https://doi.org/10.1126/science.1195320.

745 Morton, G., Nasirova, N., Sparks, D.W., Brodsky, M., Sivakumaran, S., Lambe, E.K., and Turner, E.E.
746 (2018). Chrna5-expressing neurons in the interpeduncular nucleus mediate aversion primed by prior
747 stimulation or nicotine exposure. J Neurosci 0023–18. https://doi.org/10.1523/JNEUROSCI.0023-
748 18.2018.

749 Nakayama, H., Ibañez-Tallon, I., and Heintz, N. (2018). Cell-type-specific contributions of medial
750 prefrontal neurons to flexible behaviors. Journal of Neuroscience *38*, 4490–4504.
751 https://doi.org/10.1523/JNEUROSCI.3537-17.2018.

752 Nectow, A.R., Moya, M. V., Ekstrand, M.I., Mousa, A., McGuire, K.L., Sferrazza, C.E., Field, B.C.,
753 Rabinowitz, G.S., Sawicka, K., Liang, Y., et al. (2017a). Rapid Molecular Profiling of Defined Cell
754 Types Using Viral TRAP. Cell Reports *19*, 655–667. https://doi.org/10.1016/j.celrep.2017.03.048.

755 Nectow, A.R., Moya, M. V., Ekstrand, M.I., Mousa, A., McGuire, K.L., Sferrazza, C.E., Field, B.C.,
756 Rabinowitz, G.S., Sawicka, K., Liang, Y., et al. (2017b). Rapid Molecular Profiling of Defined Cell
757 Types Using Viral TRAP. Cell Reports *19*, 655–667. https://doi.org/10.1016/j.celrep.2017.03.048.

Nichols, W.A., Henderson, B.J., Yu, C., Parker, R.L., Richards, C.I., Lester, H.A., and Miwa, J.M. (2014). Lynx1 Shifts α4β2 Nicotinic Receptor Subunit Stoichiometry by Affecting Assembly in the Endoplasmic Reticulum *. Journal of Biological Chemistry *289*, 31423–31432. https://doi.org/10.1074/JBC.M114.573667.

Ochoa, V., George, A.A., Nishi, R., and Whiteaker, P. (2016). The prototoxin LYPD6B modulates heteromeric a3β4-containing nicotinic acetylcholine receptors, but not α7 homomers. The FASEB Journal *30*, 1109–1119. https://doi.org/10.1096/FJ.15-274548.

Papke, R.L., Stokes, C., Muldoon, P., and Imad Damaj, M. (2013). Similar activity of mecamylamine stereoisomers in vitro and in vivo. Eur J Pharmacol *720*, 264. https://doi.org/10.1016/J.EJPHAR.2013.10.018.

Paxinos, G., and Franklin, K. (2004). Paxinos and Franklin's the Mouse Brain in Stereotaxic Coordinates.

Prevost, M.S., Bouchenaki, H., Barilone, N., Gielen, M., and Corringer, P.J. (2020). Concatemers to re-investigate the role of α5 in α4β2 nicotinic receptors. Cellular and Molecular Life Sciences 2020 78:3 *78*, 1051–1064. https://doi.org/10.1007/S00018-020-03558-Z.

Sadahiro, M., Demars, M.P., Burman, P., Yevoo, P., Zimmer, A., and Morishita, H. (2020). Activation of Somatostatin Interneurons by Nicotinic Modulator Lypd6 Enhances Plasticity and Functional Recovery in the Adult Mouse Visual Cortex. Journal of Neuroscience *40*, 5214–5227. https://doi.org/10.1523/JNEUROSCI.1373-19.2020.

Scholze, P., and Huck, S. (2020). The α5 Nicotinic Acetylcholine Receptor Subunit Differentially Modulates α4β2* and α3β4* Receptors. Frontiers in Synaptic Neuroscience *12*, 607959. https://doi.org/10.3389/fnsyn.2020.607959.

Schuch, J.B., Polina, E.R., Rovaris, D.L., Kappel, D.B., Mota, N.R., Cupertino, R.B., Silva, K.L., Guimarães-da-Silva, P.O., Karam, R.G., Salgado, C.A.I., et al. (2016). Pleiotropic effects of Chr15q25 nicotinic gene cluster and the relationship between smoking, cognition and ADHD. Journal of Psychiatric Research *80*, 73–78. https://doi.org/10.1016/J.JPSYCHIRES.2016.06.002.

Shenkarev, Z.O., Shulepko, M.A., Bychkov, M.L., Kulbatskii, D.S., Shlepova, O. V., Vasilyeva, N.A., Andreev-Andrievskiy, A.A., Popova, A.S., Lagereva, E.A., Loktyushov, E. V., et al. (2020). Water-soluble variant of human Lynx1 positively modulates synaptic plasticity and ameliorates cognitive impairment associated with α7-nAChR dysfunction. Journal of Neurochemistry *155*, 45–61. https://doi.org/10.1111/JNC.15018.

Sherafat, Y., Chen, E., Lallai, V., Bautista, M., Fowler, J.P., Chen, Y.C., Miwa, J., and Fowler, C.D. (2021). Differential Expression Patterns of Lynx Proteins and Involvement of Lynx1 in Prepulse Inhibition. Frontiers in Behavioral Neuroscience *15*. https://doi.org/10.3389/FNBEH.2021.703748.

Sorensen, S.A., Bernard, A., Menon, V., Royall, J.J., Glattfelder, K.J., Desta, T., Hirokawa, K., Mortrud, M., Miller, J.A., Zeng, H., et al. (2015). Correlated Gene Expression and Target Specificity Demonstrate Excitatory Projection Neuron Diversity. Cerebral Cortex *25*, 433–449. https://doi.org/10.1093/cercor/bht243.

Sparks, D.W., Tian, M.K., Sargin, D., Venkatesan, S., Intson, K., and Lambe, E.K. (2018). Opposing cholinergic and serotonergic modulation of layer 6 in prefrontal cortex. Frontiers in Neural Circuits *11*. https://doi.org/10.3389/fncir.2017.00107.

Spellman, T., Svei, M., Kaminsky, J., Manzano-Nieves, G., and Liston, C. (2021). Prefrontal deep projection neurons enable cognitive flexibility via persistent feedback monitoring. Cell *184*, 2750-2766.e17. https://doi.org/10.1016/J.CELL.2021.03.047.

Sturgeon, R.M., and Magoski, N.S. (2018). A Closely Associated Phospholipase C Regulates Cation Channel Function through Phosphoinositide Hydrolysis. Journal of Neuroscience *38*, 7622–7634. https://doi.org/10.1523/JNEUROSCI.0586-18.2018.

Sundberg, S.C., Lindström, S.H., Sanchez, G.M., and Granseth, B. (2018). Cre-expressing neurons in visual cortex of Ntsr1-Cre GN220 mice are corticothalamic and are depolarized by acetylcholine. Journal of Comparative Neurology *526*, 120–132. https://doi.org/10.1002/cne.24323.

Tasic, B., Menon, V., Nguyen, T.N., Kim, T.K., Jarsky, T., Yao, Z., Levi, B., Gray, L.T., Sorensen, S.A., Dolbeare, T., et al. (2016). Adult mouse cortical cell taxonomy revealed by single cell transcriptomics. Nature Neuroscience *19*, 335–346. https://doi.org/10.1038/nn.4216.

Tasic, B., Yao, Z., Graybuck, L.T., Smith, K.A., Nguyen, T.N., Bertagnolli, D., Goldy, J., Garren, E., Economo, M.N., Viswanathan, S., et al. (2018). Shared and distinct transcriptomic cell types across neocortical areas. Nature *563*, 72–78. https://doi.org/10.1038/s41586-018-0654-5.

Tekinay, A.B., Nong, Y., Miwa, J.M., Lieberam, I., Ibanez-Tallon, I., Greengard, P., and Heintz, N. (2009). A role for LYNX2 in anxiety-related behavior. Proc Natl Acad Sci U S A *106*, 4477. https://doi.org/10.1073/PNAS.0813109106.

Thomsen, M.S., Arvaniti, M., Jensen, M.M., Shulepko, M.A., Dolgikh, D.A., Pinborg, L.H., Härtig, W., Lyukmanova, E.N., and Mikkelsen, J.D. (2016). Lynx1 and Aβ1–42 bind competitively to multiple nicotinic acetylcholine receptor subtypes. Neurobiology of Aging *46*, 13–21. https://doi.org/10.1016/J.NEUROBIOLAGING.2016.06.009.

Thomson, A.M. (2010). Neocortical layer 6, a review. Front Neuroanat *4*, 13. https://doi.org/10.3389/fnana.2010.00013.

Tian, M.K., Bailey, C.D.C., De Biasi, M., Picciotto, M.R., and Lambe, E.K. (2011). Plasticity of prefrontal attention circuitry: upregulated muscarinic excitability in response to decreased nicotinic signaling following deletion of α5 or β2 subunits. J Neurosci *31*, 16458–16463. https://doi.org/10.1523/JNEUROSCI.3600-11.2011.

Tian, M.K., Bailey, C.D.C., and Lambe, E.K. (2014). Cholinergic excitation in mouse primary vs. associative cortex: region-specific magnitude and receptor balance. Eur J Neurosci *40*, 2608–2618. https://doi.org/10.1111/ejn.12622.

Tiong, S.Y.X., Oka, Y., Sasaki, T., Taniguchi, M., Doi, M., Akiyama, H., and Sato, M. (2019). Kcnab1 is expressed in subplate neurons with unilateral long-range inter-areal projections. Frontiers in Neuroanatomy *13*, 39. https://doi.org/10.3389/FNANA.2019.00039/BIBTEX.

Vaasjo, L.O., Han, X., Thurmon, A.N., Tiemroth, A.S., Berndt, H., Korn, M., Figueroa, A., Reyes, R., Feliciano-Ramos, P.A., and Galazo, M.J. (2021). Characterization and manipulation of Corticothalamic neurons in associative cortices using Syt6-Cre transgenic mice. Journal of Comparative Neurology https://doi.org/10.1002/CNE.25256.

836 Venkatesan, S., and Lambe, E.K. (2020). Chrna5 is essential for a rapid and protected response to
837 optogenetic release of endogenous acetylcholine in prefrontal cortex. The Journal of Neuroscience *40*,
838 7255–7268. https://doi.org/10.1523/jneurosci.1128-20.2020.

839 Venkatesan, S., Jeoung, H.-S., Chen, T., Power, S.K., Liu, Y., and Lambe, E.K. (2020). Endogenous
840 Acetylcholine and Its Modulation of Cortical Microcircuits to Enhance Cognition. In Behavioral
841 Pharmacology of the Cholinergic System, (Springer, Berlin, Heidelberg), pp. 47–69.

842 Voigts, J., Deister, C.A., and Moore, C.I. (2020). Layer 6 ensembles can selectively regulate the
843 behavioral impact and layer-specific representation of sensory deviants. Elife *9*.
844 https://doi.org/10.7554/eLife.48957.

845 Wada, E., McKinnon, D., Heinemann, S., Patrick, J., and Swanson, L.W. (1990). The distribution of
846 mRNA encoded by a new member of the neuronal nicotinic acetylcholine receptor gene family (α5) in the
847 rat central nervous system. Brain Research *526*, 45–53. https://doi.org/10.1016/0006-8993(90)90248-A.

848 Webster, J.C., Francis, M.M., Porter, J.K., Robinson, G., Stokes, C., Horenstein, B., and Papke, R.L.
849 (1999). Antagonist activities of mecamylamine and nicotine show reciprocal dependence on beta subunit
850 sequence in the second transmembrane domain. British Journal of Pharmacology *127*, 1337–1348.
851 https://doi.org/10.1038/SJ.BJP.0702686.

852 Wess, J.M., Isaiah, A., Watkins, P. V., and Kanold, P.O. (2017). Subplate neurons are the first cortical
853 neurons to respond to sensory stimuli. Proc Natl Acad Sci U S A *114*, 12602–12607.
854 https://doi.org/10.1073/PNAS.1710793114/SUPPL_FILE/PNAS.201710793SI.PDF.

855 Winzer-Serhan, U.H., and Leslie, F.M. (2005). Expression of alpha5 nicotinic acetylcholine receptor
856 subunit mRNA during hippocampal and cortical development. The Journal of Comparative Neurology
857 *481*, 19–30. https://doi.org/10.1002/cne.20357.

858 Wu, M., Puddifoot, C.A., Taylor, P., and Joiner, W.J. (2015). Mechanisms of inhibition and potentiation
859 of α4β2 nicotinic acetylcholine receptors by members of the Ly6 protein family. J Biol Chem *290*,
860 24509–24518. https://doi.org/10.1074/jbc.M115.647248.

861 Yang, D., Günter, R., Qi, G., Radnikow, G., and Feldmeyer, D. (2020). Muscarinic and Nicotinic
862 Modulation of Neocortical Layer 6A Synaptic Microcircuits Is Cooperative and Cell-Specific. Cerebral
863 Cortex *30*, 3528–3542. https://doi.org/10.1093/cercor/bhz324.

864 Yao, Z., van Velthoven, C.T.J., Nguyen, T.N., Goldy, J., Sedeno-Cortes, A.E., Baftizadeh, F.,
865 Bertagnolli, D., Casper, T., Chiang, M., Crichton, K., et al. (2021). A taxonomy of transcriptomic cell
866 types across the isocortex and hippocampal formation. Cell https://doi.org/10.1016/j.cell.2021.04.021.

867 Zolnik, T.A., Ledderose, J., Toumazou, M., Trimbuch, T., Oram, T., Rosenmund, C., Eickholt, B.J.,
868 Sachdev, R.N.S., and Larkum, M.E. (2020). Layer 6b Is Driven by Intracortical Long-Range Projection
869 Neurons. Cell Reports *30*, 3492-3505.e5. https://doi.org/10.1016/J.CELREP.2020.02.044.

870

Supplementary Material Legends

Supplementary Video 1: Video shows Chrna5+ neurons in mPFC slices from *Chrna5*-Cre$^{/+}$Ai96$^{/+}$ mice responding to exogenous application of 1mM acetylcholine with an increase in GCaMP6s fluorescence signal

Supplementary Video 2: Video shows Syt6+ neurons from *Syt6*-Cre$^{/+}$Ai96$^{/+}$ mice responding to exogenous application of 1mM acetylcholine with an increase in GCaMP6s fluorescence signal.

(Note: Supplementary Tables 1-3 are in one file)

Supplementary Table 1. Intrinsic electrophysiological properties of Chrna5+ and Chrna5- unlabeled deep-layer neurons in *Chrna5*-Cre$^{/+}$Ai14$^{/+}$ChAT-ChR2$^{/+}$ mice. None of the intrinsic properties are significantly different between the Chrna5+ and unlabeled Chrna5- neurons in Figure 1.

Supplementary Table 2. Intrinsic electrophysiological properties of Chrna5+ and Syt6+ deep-layer neurons. None of the intrinsic properties are significantly different between Chrna5+ and Syt6+ neurons in Figure 3.

Supplementary Table 3. Comparing expression of major genes modulating postsynaptic cholinergic responses in Chrna5+ and Chrna5+Syt6+ neurons. Genes of interest for cholinergic properties filtered from the list of all genes in our differential expression analysis. Genes are sorted in descending order of the fold change between Chrna5+ and Chrna5+Syt6+ neurons. 3 Lynx prototoxins- Lypd1, Ly6g6e, and Lypd6b (bold text) are the highest enriched among these cholinergic modulatory genes in Chrna5+ neurons.

Supplementary Table 4. Excel file containing all differentially expressed genes between Chrna5+ and Chrna5+Syt6+ neurons with adjusted p value < 0.05

A

Chrna5-Cre$^{/+}$
ChAT-ChR2$^{/+}$
Ai14
Chrna5-Cre$^{/+}$ Ai14$^{/+}$
ChAT-ChR2$^{/+}$

B

Chrna5+ cells ChAT axons

50 µm

C

Chrna5+ labeled L6 pyramidal neuron

10 µm

Chrna5- unlabeled L6 pyramidal neuron

D

Chrna5+ labeled
Chrna5- unlabeled
0.5 s
5 pA
20 ms
5 pA

E

Rising slope (pA/s)
800
600
400
200
0
*
Chrna5+ labeled
Chrna5- unlabeled

F

Peak current (pA)
40
30
20
10
0
*
Chrna5+ labeled
Chrna5- unlabeled

G

Chrna5-Cre$^{/+}$
Syt6-EGFP$^{/+}$
Ai14$^{/+}$
Chrna5-Cre$^{/+}$ Ai14$^{/+}$
Syt6-EGFP$^{/+}$

L6
Chrna5+
Syt6+
500 µm
Overlay

H

100 µm

I

L6
L5
L2/3
L1
Chrna5+ Syt6+ Chrna5+Syt6+
100 µm

J

% of total cells
100
80
60
40
20
0
Chrna5+
Syt6+
Chrna5+ Syt6+

Proportions of cells
37%
39%
24%
Chrna5+
Chrna5+Syt6+
Syt6+

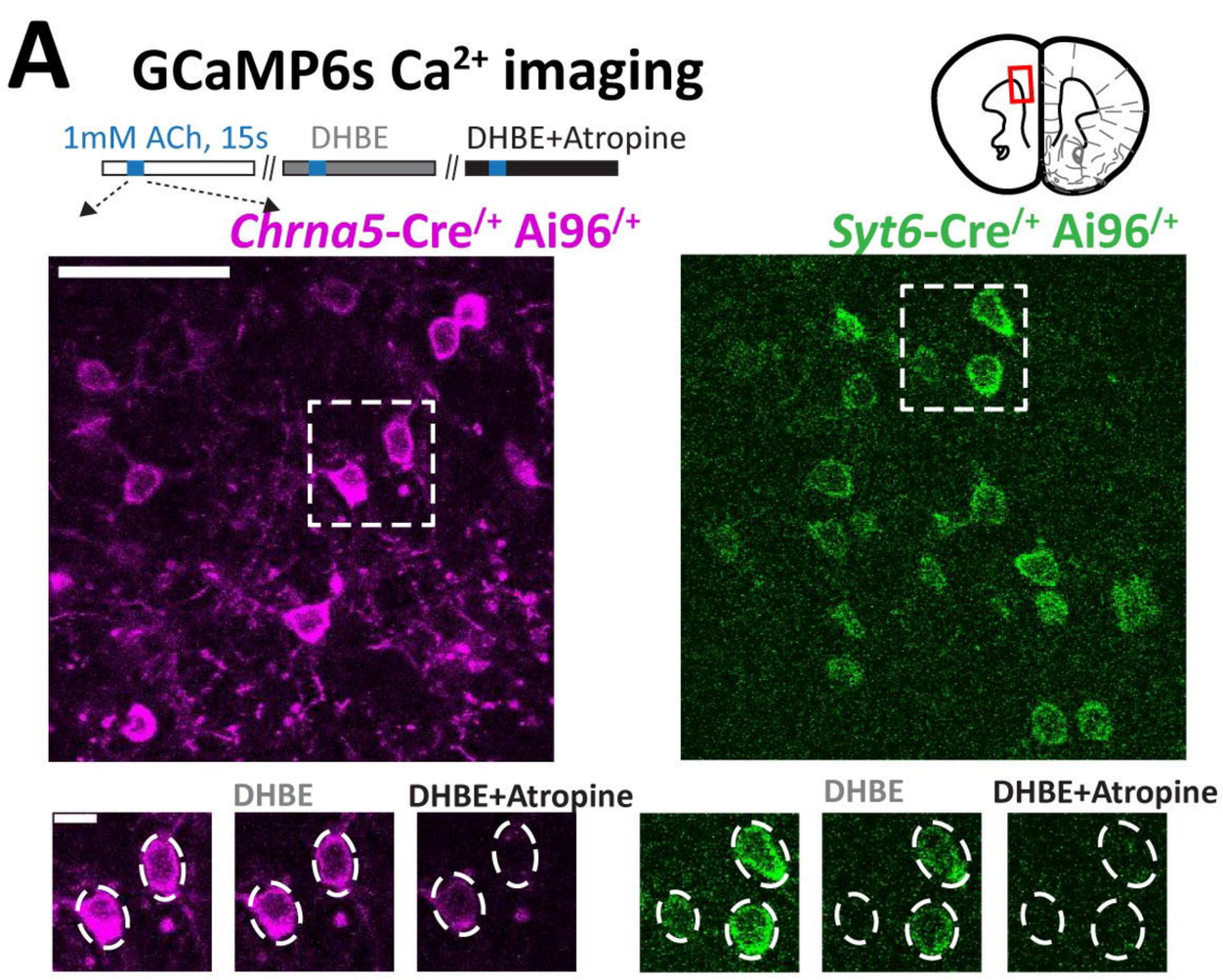

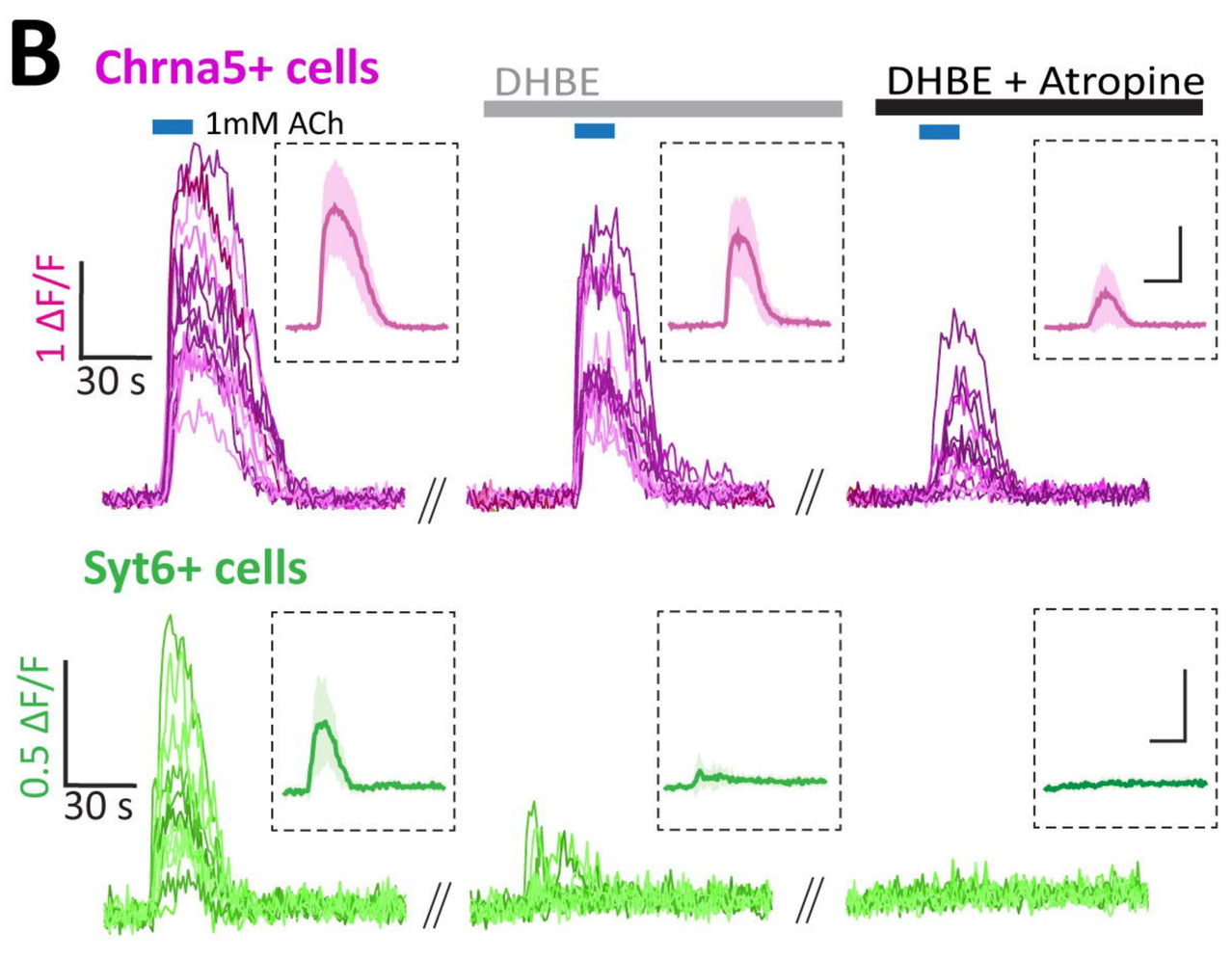

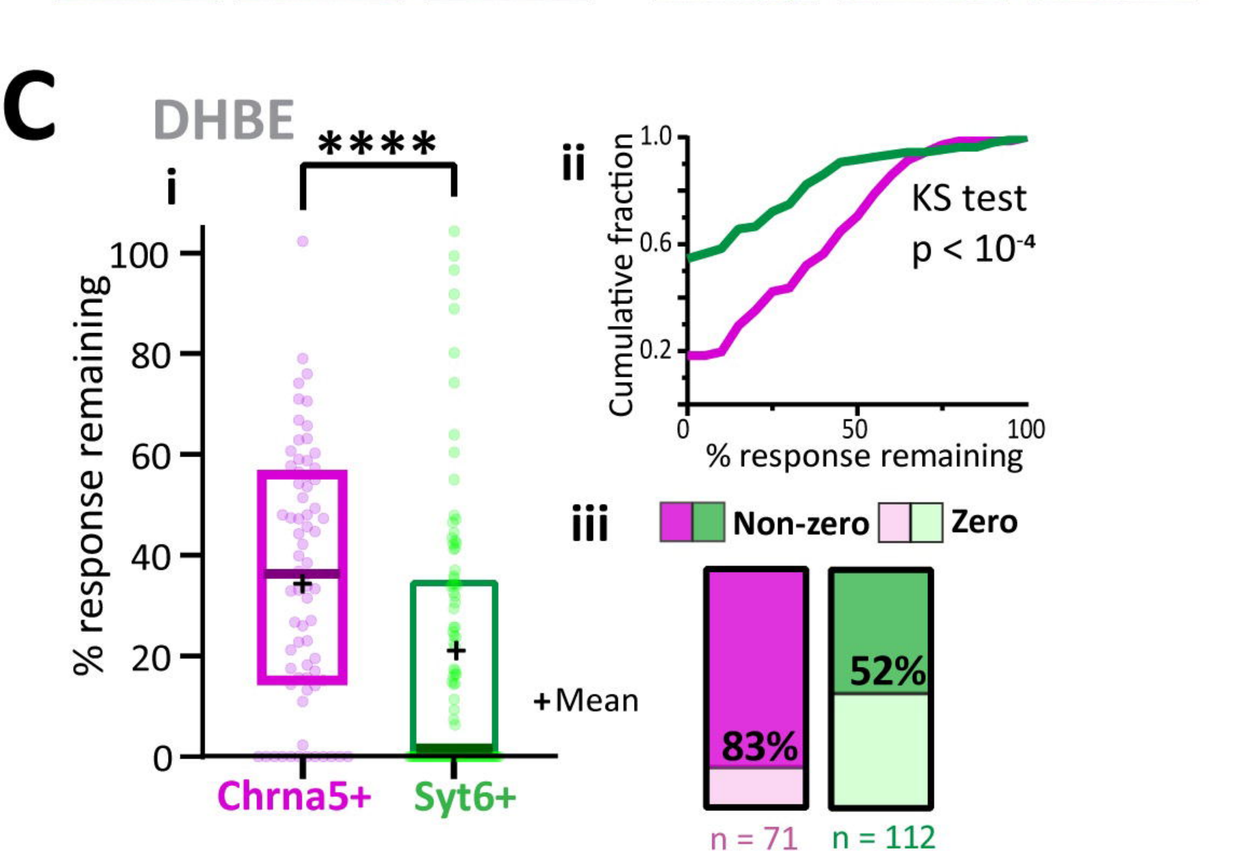

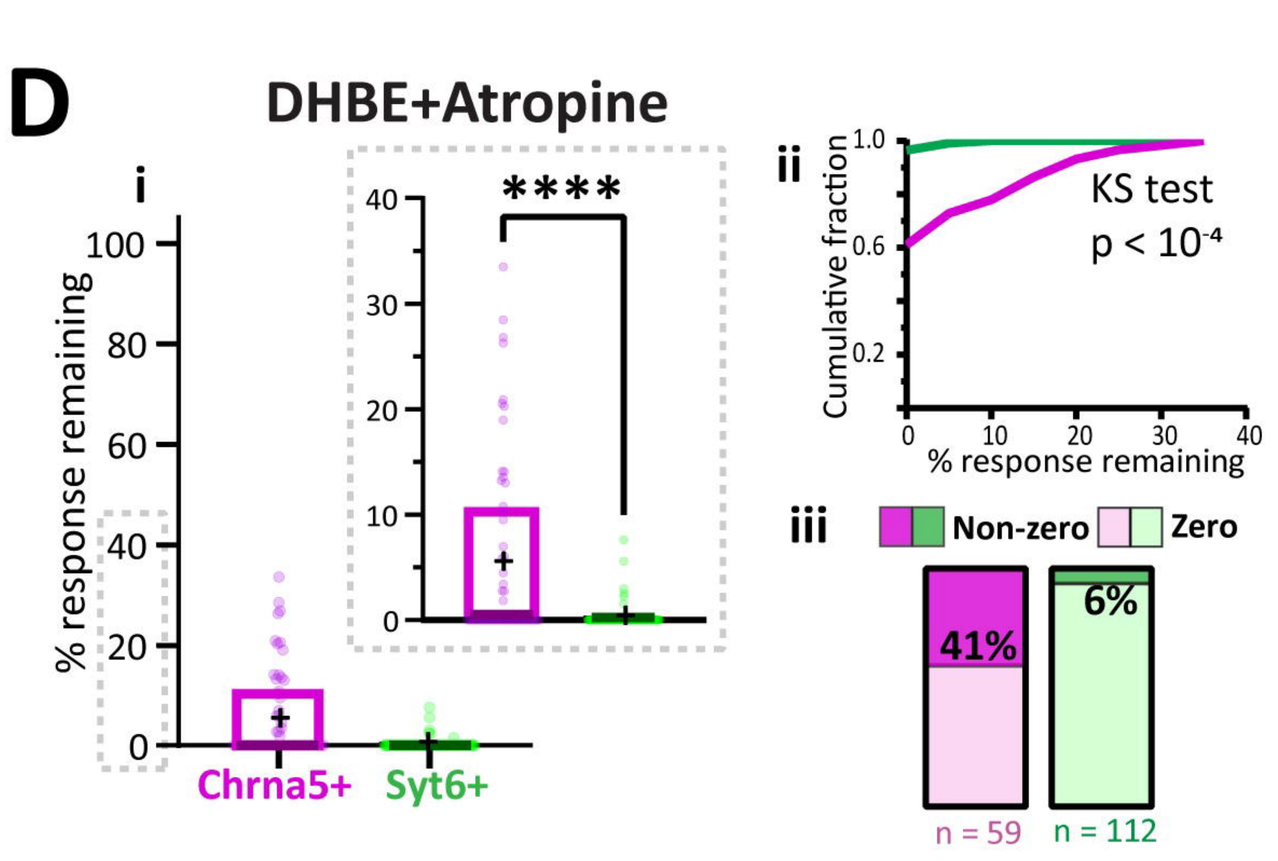

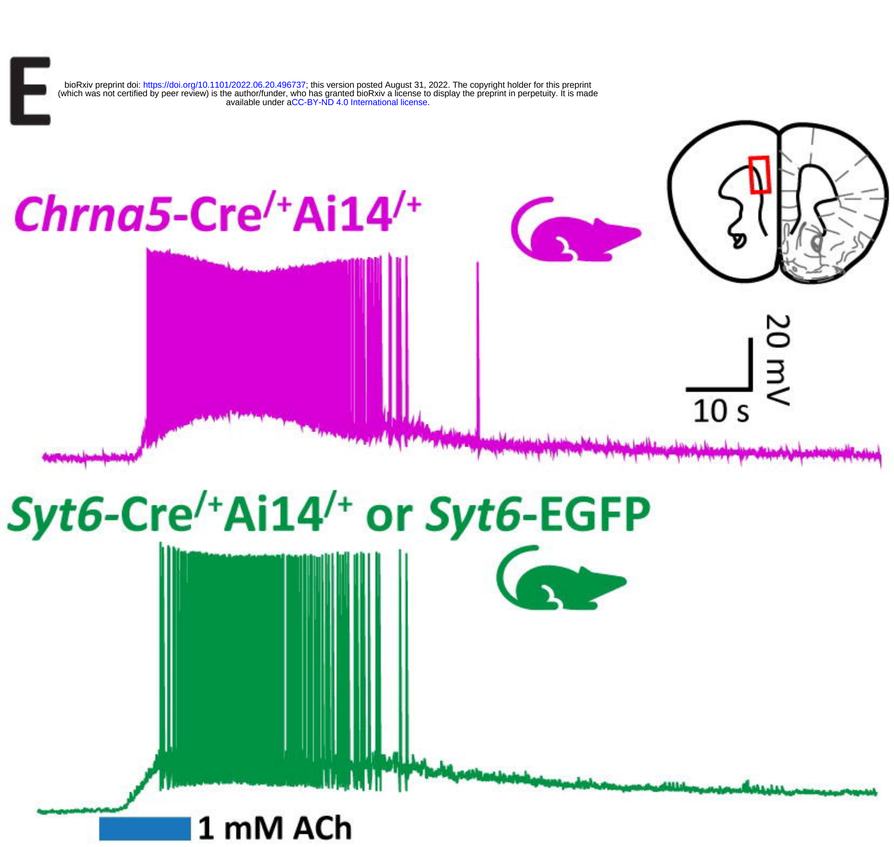

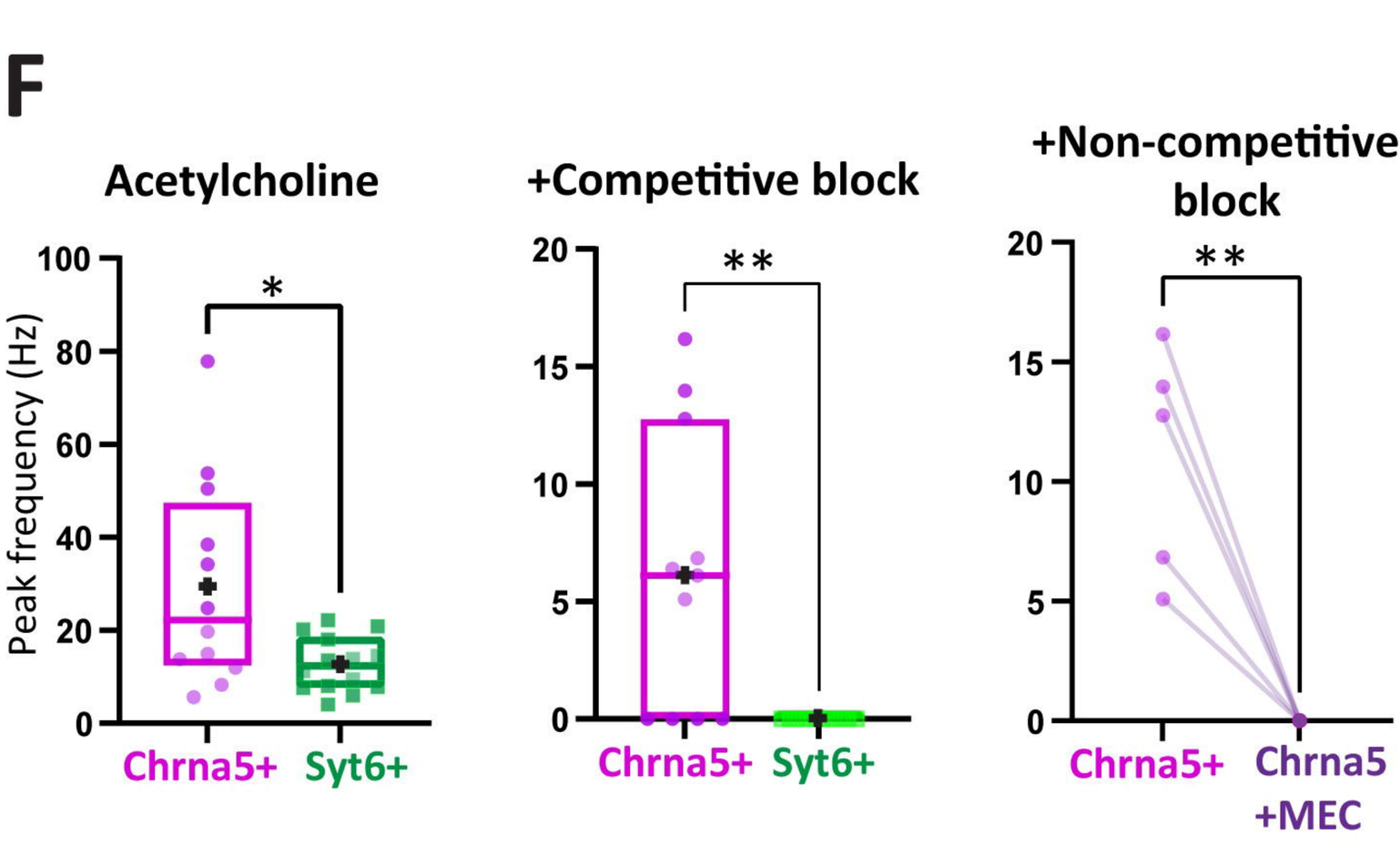

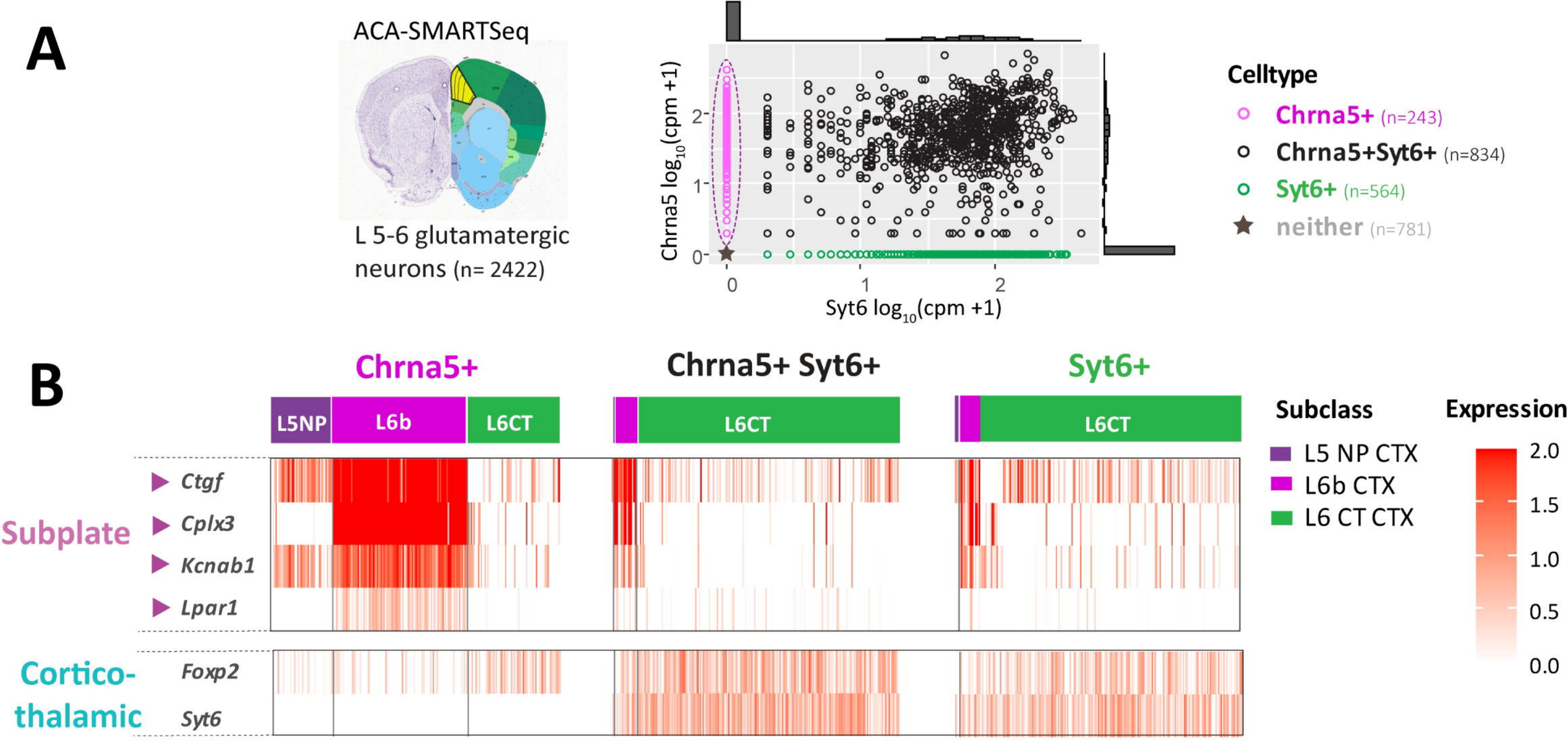

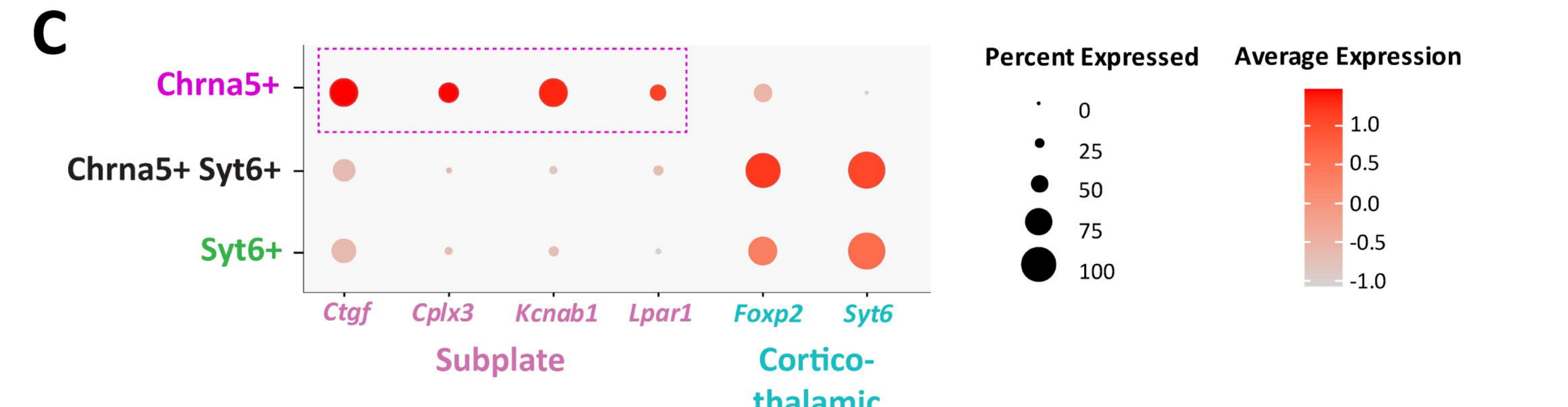

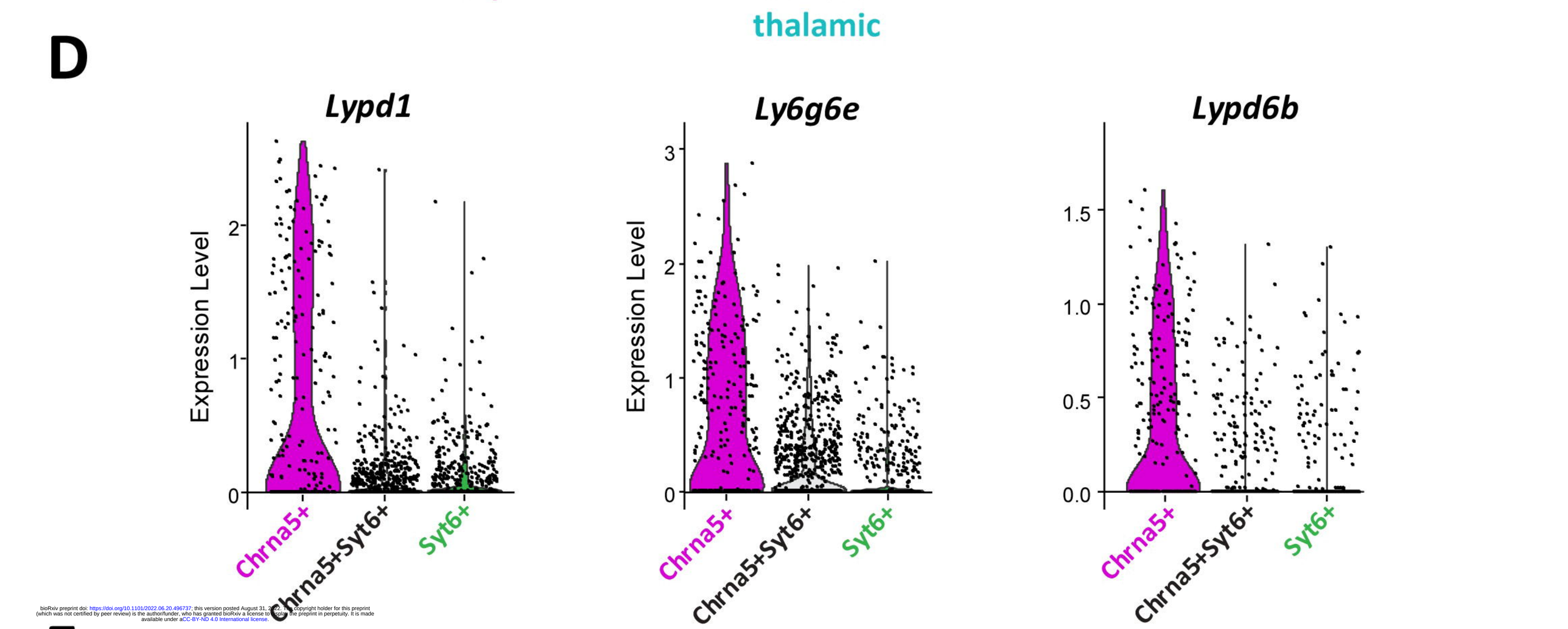

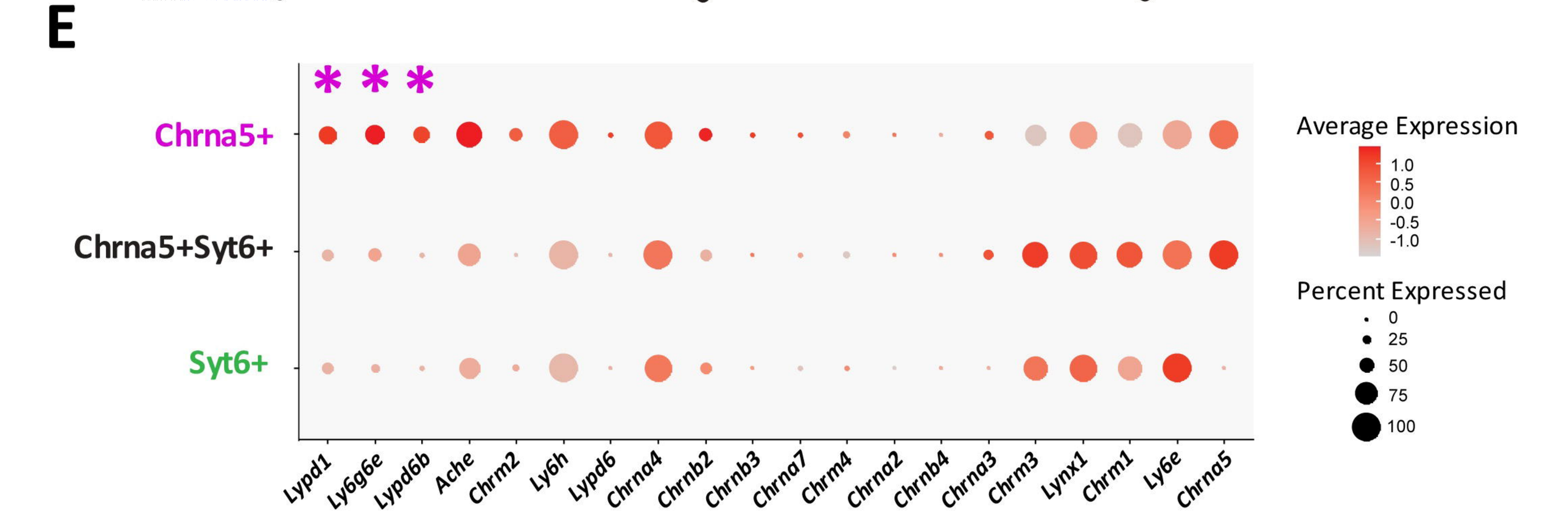

A

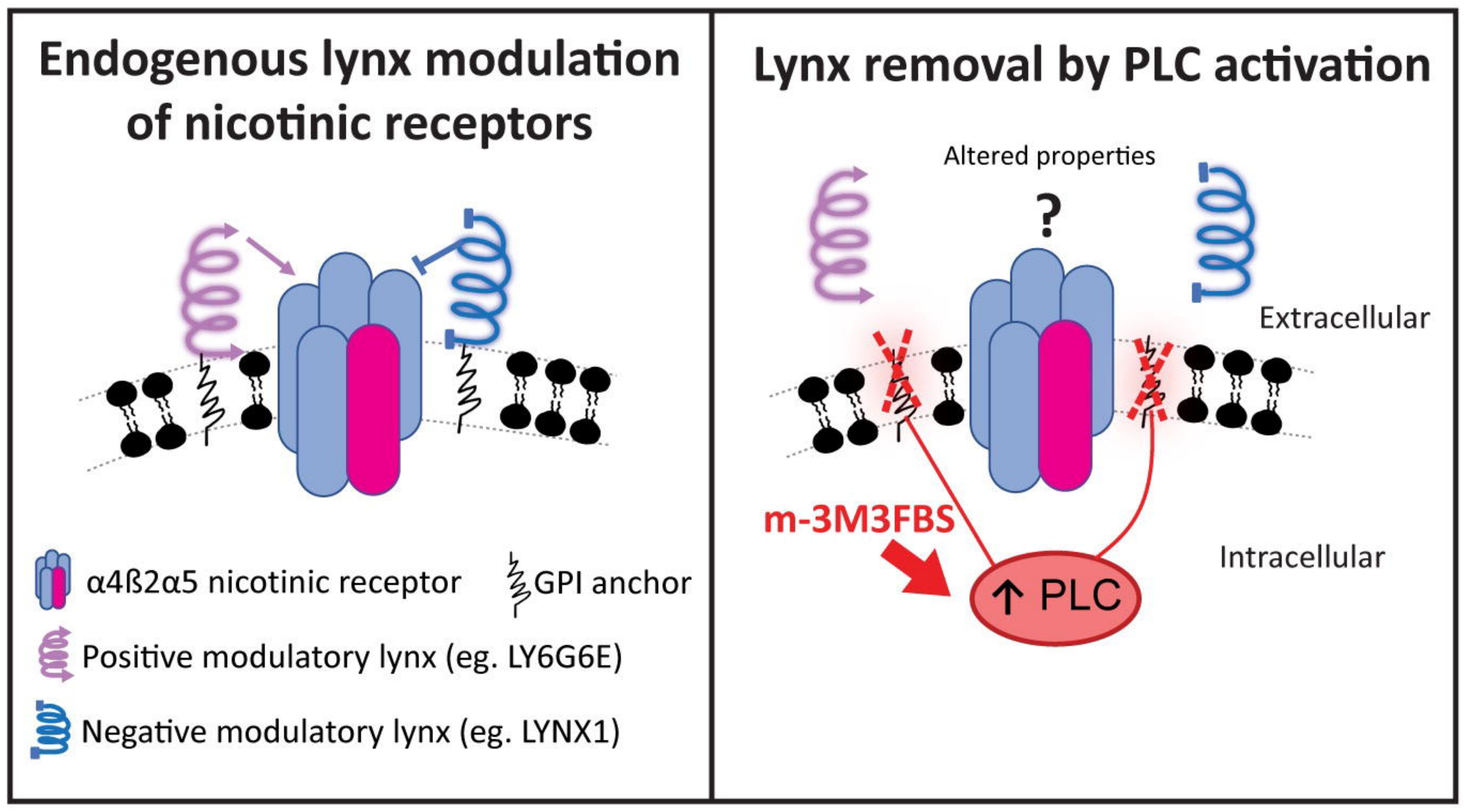

B

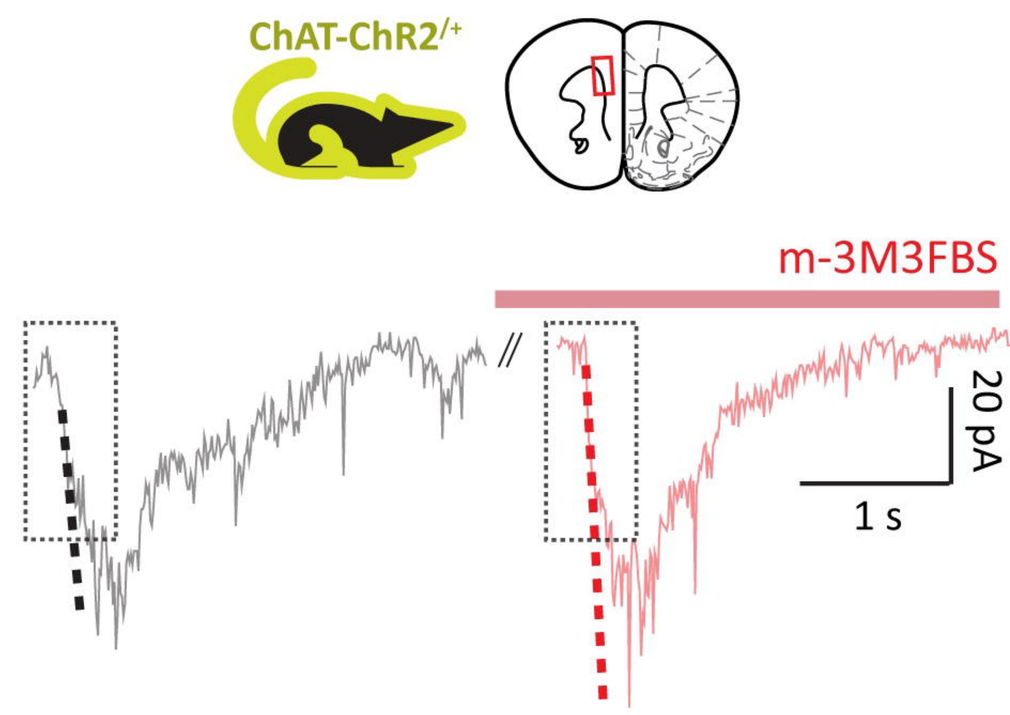

C

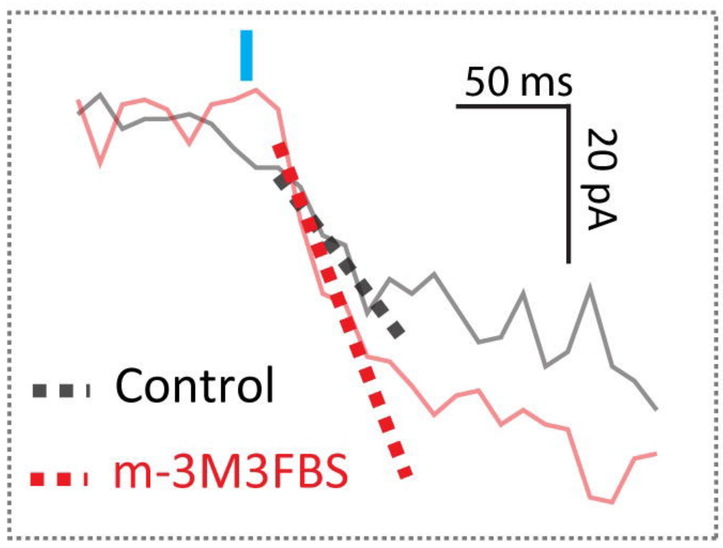

D

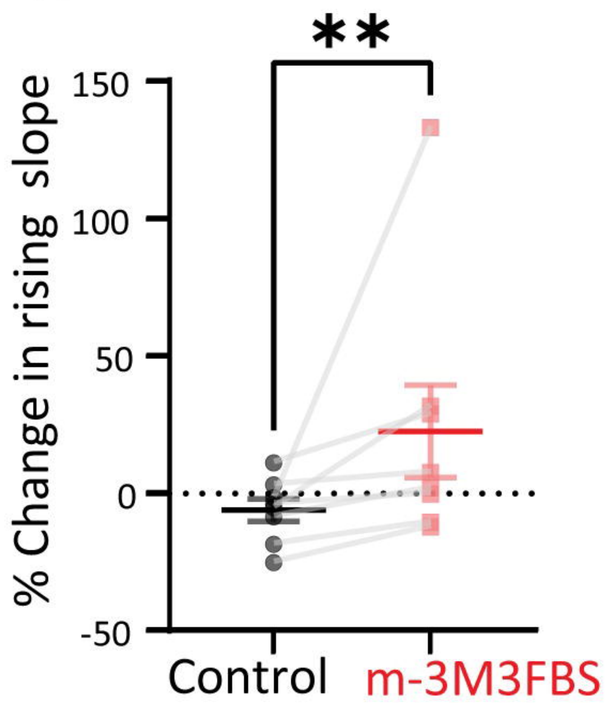

E

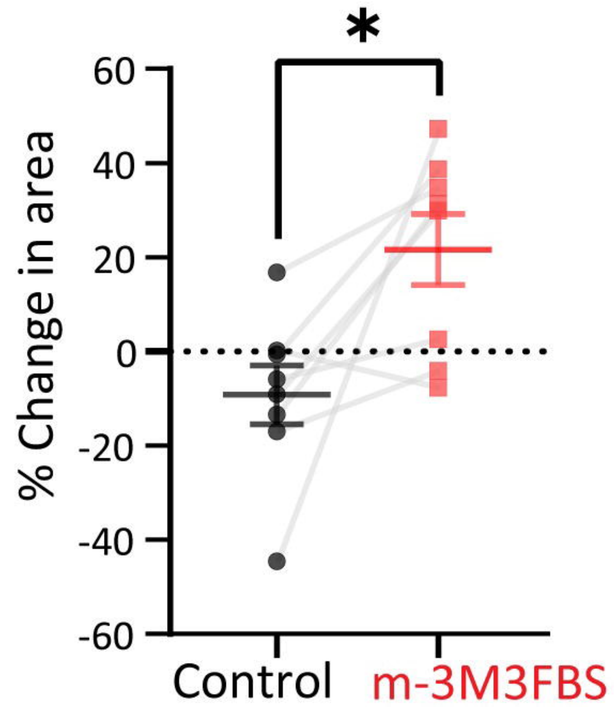

F

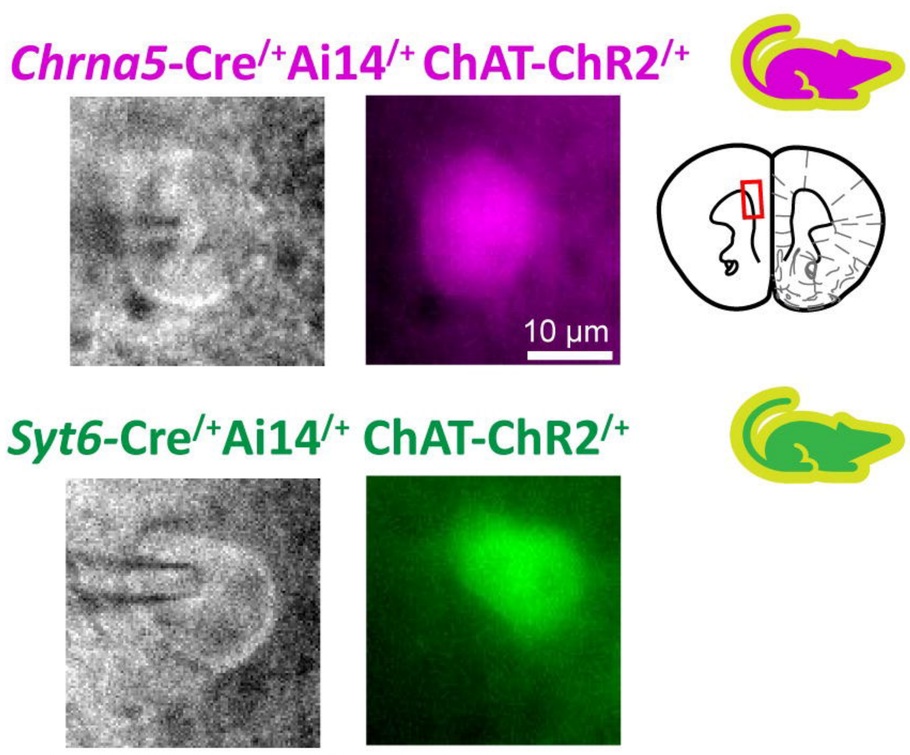

G

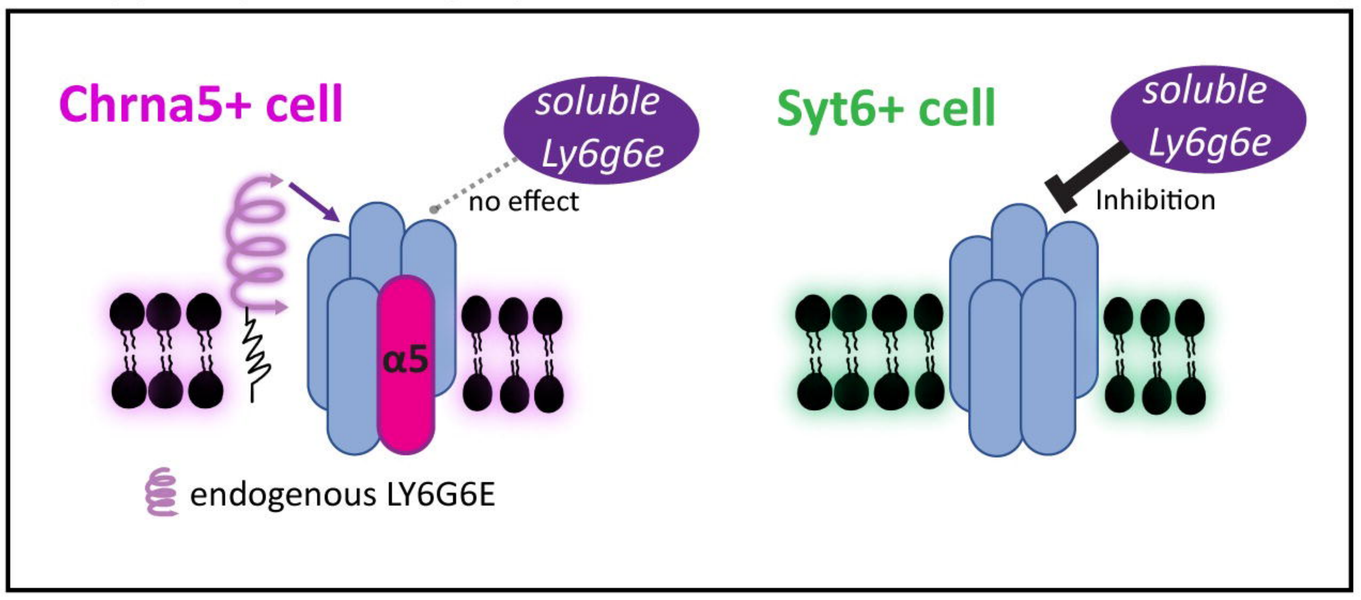

H

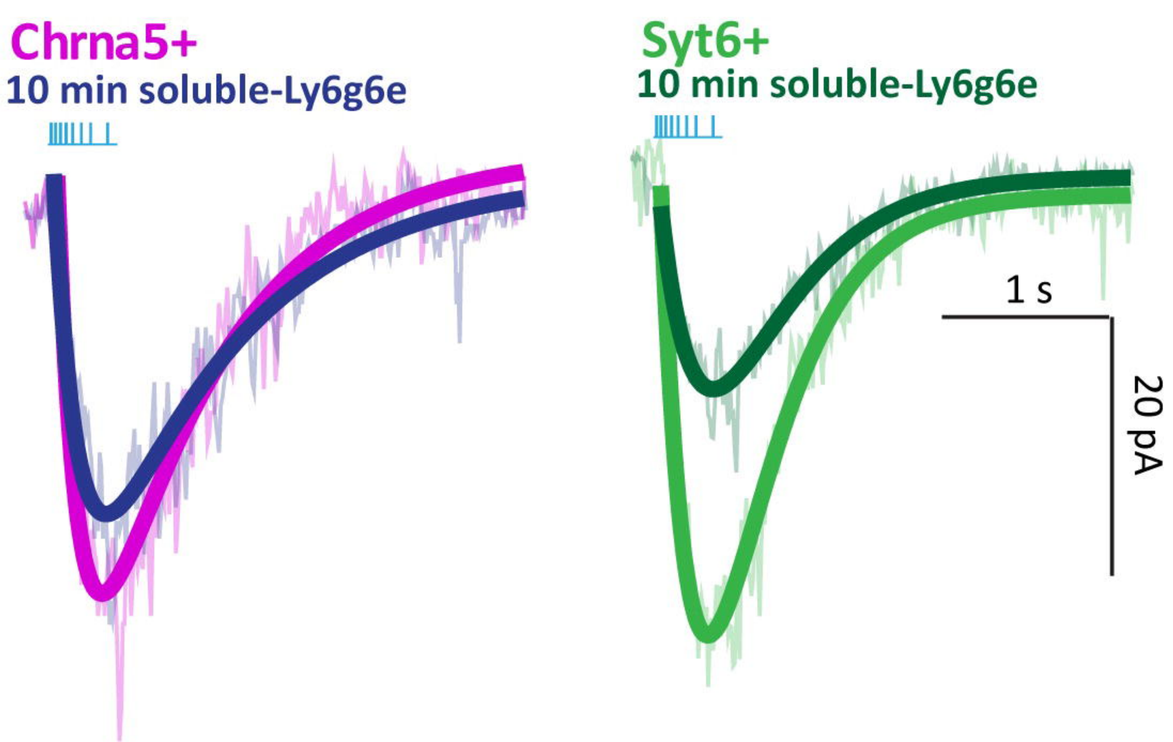

I

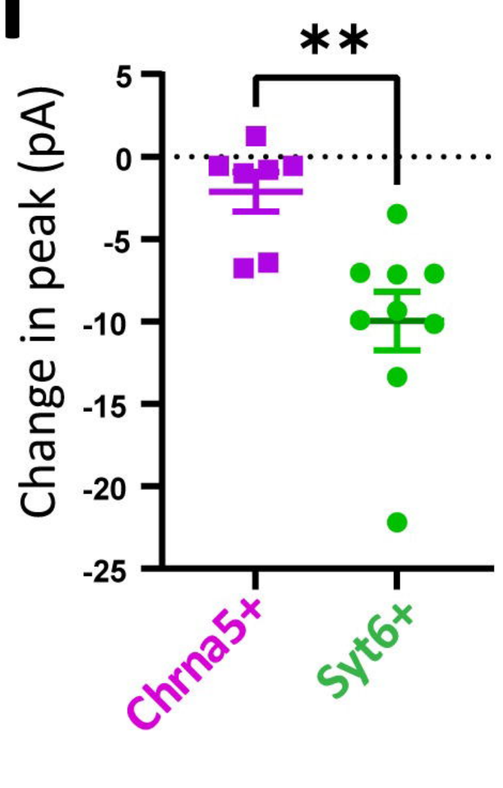

J

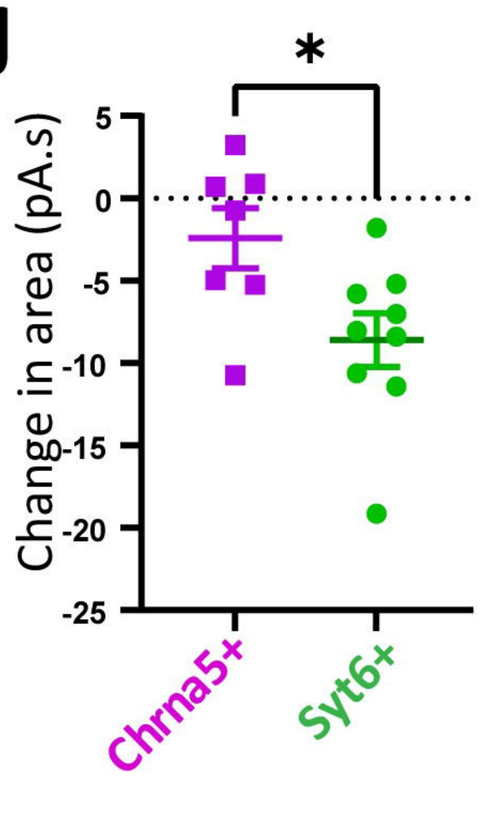

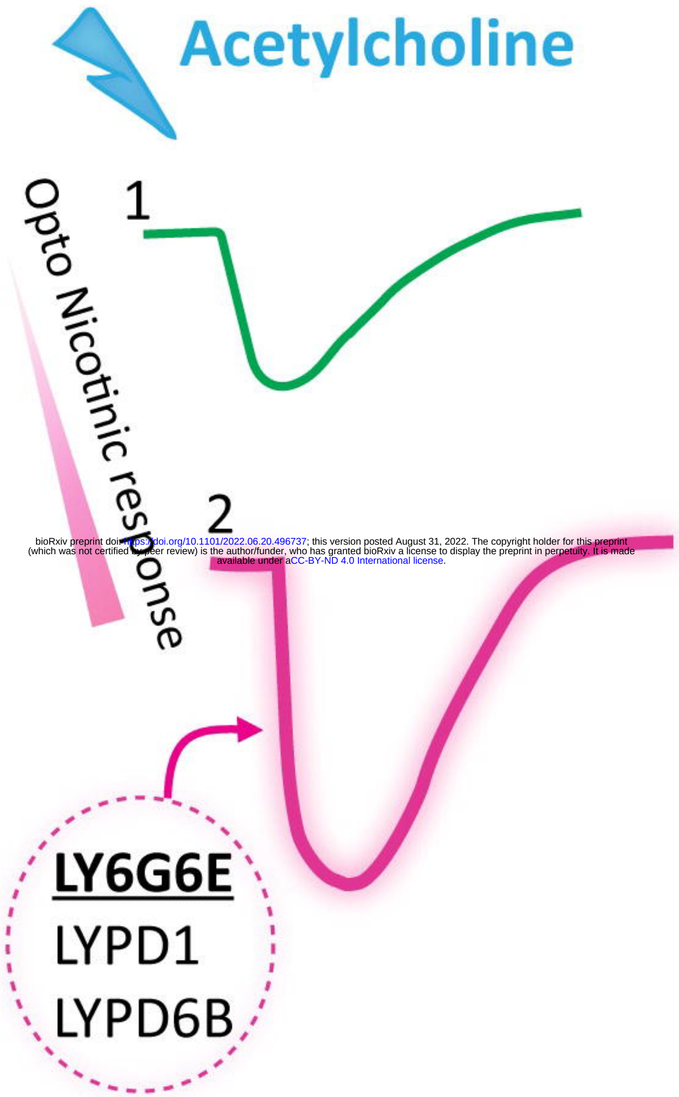

Cell-type specific Lynx modulation of nicotinic receptors

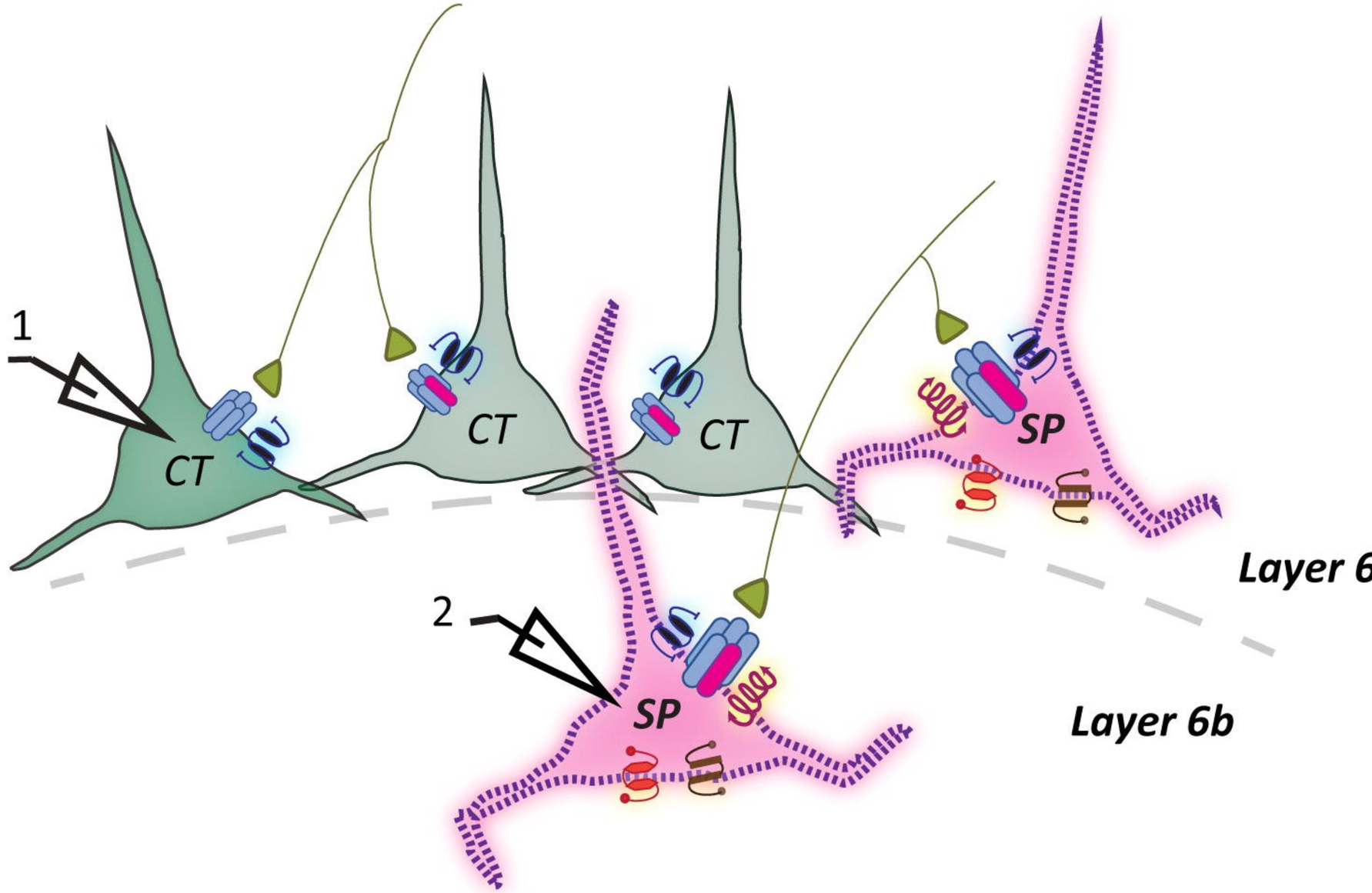

CT- Corticothalamic
SP- Subplate
Syt6+
Chrna5+Syt6+
Chrna5+

Cholinergic afferents
α4β2α5 nicotinic receptor
α4β2 nicotinic receptor

Lynx prototoxins
LY6G6E
LYNX1
LYPD6B
LYPD1 (LYNX2)